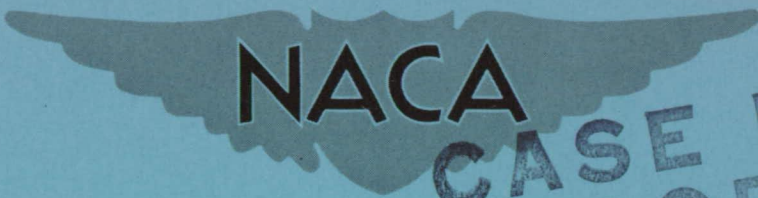


CONFIDENTIAL

Copy
RM L54B15a



**CASE FILE
COPY**

RESEARCH MEMORANDUM

AN EXPERIMENTAL INVESTIGATION OF THE
TRANSONIC-FLOW-GENERATION AND SHOCK-WAVE-REFLECTION
CHARACTERISTICS OF A TWO-DIMENSIONAL WIND TUNNEL WITH
17-PERCENT-OPEN PERFORATED WALLS

By Don D. Davis, Jr., Thomas B. Sellers, and George M. Stokes

Langley Aeronautical Laboratory
Langley Field, Va.

CLASSIFICATION CHANGED TO UNCLASSIFIED

AUTHORITY: NACA RESEARCH ABSTRACT NO. 97

DATE: FEBRUARY 24, 1956

WH L

CLASSIFIED DOCUMENT

This material contains information affecting the National Defense of the United States within the meaning of the espionage laws, Title 18, U.S.C., Secs. 793 and 794, the transmission or revelation of which in any manner to an unauthorized person is prohibited by law.

NATIONAL ADVISORY COMMITTEE FOR AERONAUTICS

WASHINGTON

April 26, 1954

CONFIDENTIAL

NATIONAL ADVISORY COMMITTEE FOR AERONAUTICS

RESEARCH MEMORANDUMAN EXPERIMENTAL INVESTIGATION OF THE
TRANSONIC-FLOW-GENERATION AND SHOCK-WAVE-REFLECTION
CHARACTERISTICS OF A TWO-DIMENSIONAL WIND TUNNEL WITH
17-PERCENT-OPEN PERFORATED WALLS

By Don D. Davis, Jr., Thomas B. Sellers, and George M. Stokes

SUMMARY

The transonic-flow-generation and shock-wave-reflection characteristics of a test section with 17-percent-open perforated top and bottom walls have been investigated in a 3- by 3-inch transonic flow apparatus. A test section of acceptable flow uniformity was obtained through the Mach number range (0.80 to 1.3). Wall divergence was used to eliminate a velocity gradient near a Mach number of 1.3.

Wave-reflection tests were made with the perforated walls diverged at angles of 10', 15', 20', 25', and 30' at a free-stream Mach number of 1.28 with a Mach number decrement across the leading-edge shock of 0.09. With the walls diverged 25', the wall-divergence and wall-porosity characteristics combined to allow the flow near the wall to turn to the correct (interference-free) direction after passing through the region near the shock wave, but a disturbance was reflected from the region of turning. This disturbance consisted of a compression followed by an expansion and then by a second compression. The disturbance, which was present at all divergence angles in excess of 10', was weaker and affected a smaller portion of the model than the disturbance reflected from a deep, multi-slotted wall tested previously (NACA RM L53J28). This disturbance was found to be caused by the shock-wave boundary-layer interaction. It was possible to prevent the boundary layer from thickening far upstream of the incident shock if the wall divergence was decreased to 10'. In this case, the boundary-layer displacement thickness just upstream of the shock was about 0.008 inch. With the divergence decreased to 10', however, a shock was reflected from the wall, indicating that the flow through the wall had decreased. The outflow decrease is related to decreases in boundary layer thickness and rate of growth which are caused by the decrease in divergence.

Perforated-wall boundary-layer surveys and suction mass-flow measurements were made at a Mach number of 0.98 over a wall-angle range from 15' converged to 30' diverged. Also, equations were derived which related the suction flow to the boundary layer and the effective wall friction coefficient.

INTRODUCTION

The problem of the reflection of shock waves from various types of porous walls is being investigated in a 3- by 3-inch transonic flow apparatus located in the Langley full-scale tunnel. In reference 1 the results of an investigation of transonic-flow generation and shock-wave reflection with slotted walls with very deep narrow slots have been presented. The reflected disturbance was found to be much different from that predicted from simple nonviscous flow considerations. Whereas a nonviscous flow adjacent to a wall of uniform porosity would be expected to give a single reflected disturbance (compression or expansion, depending on the porosity) followed by a region of constant pressure, the experiment showed a compression followed by an expansion and then by a long region of compression. The constant pressure region did not materialize.

The initial compression-expansion disturbance was thought to result from a forward travel of the high-pressure field from behind the shock through either the boundary layer or the deep slots or both. In order to study this problem further, a pair of perforated walls was constructed. Perforated walls were chosen in order to eliminate the possibility of forward travel of the pressure field inside the walls themselves so that the effect of the boundary layer could be studied separately. The wall divergence was made variable in order that the boundary-layer thickness could be varied during the investigation. This paper presents the results of two-dimensional wave-reflection tests made at a Mach number of 1.28 in the perforated-wall test section.

The characteristics of the perforated wall in a transonic flow nozzle were also investigated and are reported herein. Also presented are results of a boundary-layer investigation showing the relationship between the suction mass flow, the rate of growth of the boundary layer, and the wall friction coefficient.

SYMBOLS AND COEFFICIENTS

C_f	effective wall friction coefficient
h	tunnel height
H	boundary-layer shape parameter, δ^*/θ
H_1	total pressure in tunnel upstream of test section
H_2	total pressure indicated by impact tube (uncorrected for shock losses)

l	length of porous test section
M	Mach number
ΔM	decrement in Mach number across incident shock wave
m	total mass flow in tunnel throat
Δm	suction mass flow
P	static pressure
Re_{θ}	Reynolds number, $\frac{\rho_{\delta} U_{\theta}}{\mu}$
u	velocity in boundary layer
U	free-stream velocity
V	free-stream velocity component normal to wall
w	tunnel width
x	axial distance from reference point
y	vertical distance from reference plane
ρ_{δ}	free-stream density, slugs/ft ³
ρ	density in boundary layer, slugs/ft ³
δ^*	boundary-layer displacement thickness
δ	boundary-layer thickness
θ	boundary-layer momentum thickness
γ	perforated-wall divergence angle, minutes
μ	coefficient of viscosity, slugs/ft-sec
$\rho_0 v_0$	suction mass flow per unit porous wall area

Subscripts:

p	porous wall
s	solid wall

EQUIPMENT AND APPARATUS

Test Section

The basic equipment and apparatus used in this investigation are described in reference 1. For the present investigation, the removable two-dimensional test section was fitted with top and bottom walls made of perforated aluminum sheet. The material used was commercial grade, 17-percent-open, 0.032-inch-thick, aluminum sheet with 0.027-inch-nominal-diameter holes. There were 303 holes per square inch with the centers of the holes 0.0664 inch apart in a 60° staggered arrangement (fig. 1). The tunnel throat area and the total perforated wall area of the test section were 8.93 and 65.26 square inches, respectively, with the tunnel walls parallel.

Because the information of reference 2 regarding the parallel flow porosity characteristics of perforated walls was not available at the time these walls were built, they were made with a constant open ratio from front to rear. Flow overexpansion near the front was known to be characteristic of constant open-ratio slotted walls; therefore, provision was made for closing off some of the holes in the perforated walls in case overexpansion was encountered.

The perforated sheet wall configuration extended from station $-\frac{5}{16}$ to station $13\frac{1}{8}$ with the perforations open to the plenum tanks from station 0 to station $10\frac{13}{16}$. In order to hold the perforated sheets securely in place and still leave the maximum number of perforations open, the aluminum sheet was supported by four longitudinal knife edges. The two center knife edges were bonded to the aluminum sheet from station 0 to station 6. The bonding material closed approximately two longitudinal rows of perforations along each of the two center knife edges, but in the test region the bonding material was omitted and all the perforations were open in the region extending from station 6 to station $10\frac{13}{16}$.

The perforated sheet wall was formed with two longitudinal flanges along the length of the perforated wall. These flanges of the perforated sheet were clamped between the outside knife edges and the side rails. The radius at the corner where the flanges were formed was kept to a minimum (approximately $1/32$ inch). As is shown in figure 1, there was a 0.030-inch-wide slot along each side of the tunnel. The purpose of these slots was to remove the boundary layer in the corners of the tunnel. Several $1/4$ -inch-diameter holes, which were located on each side and along the length of the perforated wall, made possible the transfer of air from the slots to the plenum tanks. The wall-divergence mechanism

described in reference 1 was unaltered, but the wall side rails were altered by tapering them sufficiently to allow a maximum wall-angle range from 60' converged to 60' diverged (see fig. 1). Photographs of the test section installation are presented in figure 2.

Probes

The center-line static-pressure probe and the movable static-pressure probe that were described in reference 1 were used in this investigation. In addition, a boundary-layer probe was used. This probe was mounted in the same manner as the movable static-pressure probe and could be moved vertically and axially. The probe was supported by a 1/4-inch-diameter rod similar to the movable-static-probe arrangement. The boundary-layer probe was made up of a center static-pressure tube with two total pressure tubes located 3/8 inch above and below the center static tube (see fig. 3). The center static tube was identical to the static-pressure tube of the movable static probe. The total-pressure tubes were made of 0.020-inch-outside-diameter stainless-steel tubing with 0.010-inch inside diameter. This tubing was flattened until a 0.002-inch-high and 0.010-inch-long opening was formed at the end of the tube. The outside height of the tube was ground down to 0.007 inch. The probe could be positioned vertically to within ± 0.001 inch. For boundary-layer surveys in the forward part of the test section, a similar probe was mounted on a longer 1/4-inch rod which was supported behind station $8\frac{1}{8}$ by a larger rod which tapered in outside diameter from 1/2 inch at the diffuser entrance to 3/8 inch at station $8\frac{1}{8}$.

Model

The model was a semidiamond two-dimensional airfoil with a chord of 3 inches and an included apex angle of 5° at the leading and trailing edges. Nine flush static-pressure orifices were located at 10-percent-chord intervals on the flat lower surface. The leading edge of the model was located at station $8\frac{1}{8}$. The model was mounted in the tunnel by shafts which extended from the 50-percent-chord point. These shafts were fitted into holes drilled through the glass side wall. The cross-sectional shape of the model including the shaft is shown in figure 1. The model mounting procedure is described in reference 1.

TESTS

These tests were conducted with a tunnel stagnation pressure and temperature of approximately one atmosphere and 200° F, respectively.

Center-Line Mach Number Distributions

Center-line Mach number distributions were obtained with the perforated walls parallel at Mach numbers from 0.8 to 1.3 and with the perforated walls diverged 30' at a Mach number of 1.3. The center-line Mach numbers were determined from the static pressures measured with the center-line static probe and the tunnel total pressure measured upstream of the test section.

Boundary-Layer Surveys, Tunnel Empty

Surveys of the total and static pressures in the perforated-wall boundary layer were obtained with the boundary-layer probe. These surveys were taken at wall divergence angles of -15', 0', 15', and 30' at station $10\frac{1}{2}$ at $M = 1.28$ and at stations 1 and $10\frac{1}{2}$ at $M = 0.98$. As was pointed out in the preceding section, an extension to the movable-probe assembly was necessary in order to survey the boundary layer at station 1. Therefore, the boundary layer was measured first at station 1 at the various wall divergence angles. Then, the probe extension was removed and the boundary layer was measured at station $10\frac{1}{2}$ at the same divergence angles.

Suction Measurements

Measurements of the mass of air removed by suction through the 17-percent-open perforated walls at a Mach number of 0.98 at divergence angles of -15', -10', 0', and 15' were obtained with a calibrated orifice plate located in the 6-inch-diameter duct which connected the plenum tanks to the suction supercharger.

Wave-Reflection Tests

The test region wherein the model was mounted extended from station $8\frac{1}{8}$ to station $11\frac{1}{8}$. In the wave-reflection tests, a free-stream Mach number of 1.28 was held constant, and at each wall-divergence-angle setting the model angle of attack was adjusted to maintain a constant Mach number decrement (ΔM) of 0.09 across the model leading-edge shock between the lower model surface and the tunnel wall. The resulting angle of attack of the model was such that the flow deflection angle produced by the upper surface was greater than that produced by the lower surface. The wall divergence angle was varied through the range from 10' to 30'. The movable static probe was used in the wave-reflection

tests to obtain the longitudinal static-pressure surveys, which were taken along lines $1/2$, $3/4$, and $1\frac{3}{8}$ inches below the tunnel center line.

For the case of $20'$ wall divergence, the flow was surveyed only along a line $1/2$ inch below the tunnel center line. The static pressure surveys extended from the flow region upstream of the incident shock to a point well downstream of the wall-reflected disturbance.

Boundary-Layer Surveys, Model in Tunnel

With the model mounted in the tunnel, boundary-layer surveys were made in the vicinity of the shock-boundary-layer intersection at wall divergence angles of $10'$ and $20'$. These surveys were made at four longitudinal positions ranging from 1 inch ahead to $1/16$ inch behind the shock-boundary-layer intersection, which was located at about station 9.

RESULTS AND DISCUSSION

Flow Generation

In order to investigate the development of flow in the perforated nozzle and test section, axial-center-line static-pressure surveys were made at several Mach numbers ranging from 0.8 to 1.3. Figure 4 presents Mach number distributions for the region extending from $x = -2$ to $x = 11\frac{1}{4}$ inches in $1/4$ -inch intervals. The perforations are open from $x = 0$ to $x = 10\frac{13}{16}$ inches.

Perforated Walls Parallel

Figure 4 shows that with the walls parallel the flow is quite uniform in the subsonic case with an essentially constant Mach number between $x = 0$ and $x = 10\frac{3}{4}$ inches. In the supersonic range the maximum Mach number deviation is ± 0.002 for the $M = 1.01$ case from $x = 1$ to $x = 10.5$ inches and ± 0.005 for the $M = 1.11$ case from $x = 2.5$ inches to the end of the test section. As the supersonic Mach number is increased above 1.11, the distance required for the generation of the supersonic flow in the front or nozzle portion of the test section increases. In addition, a velocity gradient appears in the test region from $x = 8\frac{1}{8}$ to $11\frac{1}{8}$ inches. This gradient is too small to be of much significance

except at the highest Mach number, where it approaches 0.02 per tunnel height. Furthermore, it will be shown that the gradient can readily be eliminated by diverging the walls slightly. The presence of the gradient indicates that the perforated wall is too dense to allow the flow to accelerate to the final equilibrium Mach number in the available tunnel length. The smooth velocity distribution obtained at a Mach number of 1.11 contrasts sharply with the oscillating-type distribution that was encountered at about the same Mach number with the deep slotted walls of reference 1. Inasmuch as no serious overshoot was encountered, it was not necessary to close any of the holes near the front of the perforated wall.

A schlieren photograph showing the field of flow in the test section is presented in figure 5(a). Note that the disturbance lines which emanate from the holes in the perforated wall can be traced across the tunnel. Attempts to measure the pressure rise across a single disturbance were unsuccessful because of the size of the pressure probe, so the strength of these disturbances is not known.

Effect of Wall Divergence

The walls were diverged 30' at a Mach number of 1.28 in order to study the effect of wall divergence on the flow generation and on the acceleration in the test region ($x = 8\frac{1}{8}$ to $x = 11\frac{1}{8}$ inches). The results presented in figure 4 show that the acceleration was eliminated. An essentially uniform flow (± 0.004) is reached at $x = 6$ inches, two test-section heights from the front of the perforated wall. The increased flow velocity in the solid-wall subsonic-nozzle region ahead of $x = 0$ is a result of the movement of the solid walls (the flexure plates) which accompanies the change in wall divergence (see ref. 1).

A schlieren photograph of the flow field for 30' divergence at a Mach number of 1.28, which was made with a horizontal knife edge, is presented in order to show the more rapid development of the boundary layer with the walls diverged (fig. 5(b)). This is a portion of a photograph which was made with the model installed; consequently, it has been cut off at about $x = 8$ inches. It is interesting to note also that, as the boundary layer thickens downstream, the disturbances from the holes in the perforated walls become less prominent. The boundary-layer displacement thickness in the region near $x = 8$ inches is roughly equal to the hole diameter.

Boundary-Layer Surveys

Effect of wall divergence at $M = 0.98$. Boundary-layer surveys were made to determine the thickness and the rate of growth of the boundary

layer on the perforated wall at several divergence angles at a Mach number of 0.98. The boundary-layer displacement thickness determined from these surveys is plotted as a function of the wall divergence in figure 6. The average rate of increase of the boundary-layer displacement thickness as determined from these measurements is plotted in figure 7 as a function of the wall divergence angle. The value of $d\delta^*/dx$ increased from 0.00048 at $\gamma = -15'$ to 0.00570 at $\gamma = 30'$. The boundary-layer velocity profiles were of the type which is generally associated with turbulent boundary layers.

Effect of wall divergence at $M = 1.28$.- The boundary-layer displacement thickness at $x = 10.5$ inches is plotted as a function of the wall divergence angle in figure 8 for a Mach number of 1.28. Diverging the walls caused δ^* to increase from about 0.0054 at $\gamma = -15'$ to about 0.0280 at $\gamma = 30'$. Variation of the wall divergence angle is thus seen to be an effective means of varying the boundary-layer thickness.

Shock-Wave Reflection

Static-pressure surveys.- The results of axial static-pressure surveys in the flow field between the model and the tunnel wall are presented in figure 9. In order to present these results more graphically, the data for the axial surveys have been plotted with the scales displaced in such a manner that the lines $P/H_1 = 0.42$ are located at vertical positions which correspond approximately to the vertical stations along which the surveys were made. The model pressures are plotted with the line $P/H_1 = 0.42$ in a position which corresponds to the center line of the tunnel. This type of plot enables the viewer to trace a compression or expansion wave through the flow.

At a wall divergence angle of $10'$, the shock wave is reflected as a compression wave (fig. 9(a)), indicating that at this condition, the wall was too dense and the outflow through the wall behind the shock wave was not sufficient to prevent the reflection. Note, however, that the reflected compression is much weaker than the incident shock wave. As the wall divergence angle is increased to $15'$ (fig. 9(b)), the flow near the wall is able to turn through a larger angle resulting in a further reduction in the strength of the reflected wave. This process continues as the wall divergence is increased until a point is reached where with further increase of divergence the reflection becomes mainly an expansion wave that increases in strength as the divergence is further increased. The boundary-layer behavior is connected with the fact that the flow turns through larger angles as the divergence is increased. As the divergence is increased the initial outflow ahead of the shock is decreased, while the pressure outside the wall is slightly increased. At the same time the boundary-layer thickness is increased, which results in a decrease in velocity in the region near the wall. The calibration

results of reference 2 show that this decrease in velocity will result in an increased outflow. The increased outflow behind the shock and the decreased outflow ahead of the shock combine to cause the flow to turn through a larger angle as the divergence is increased.

At a divergence of 25' (fig. 9(d)), the flow survey taken 0.5 inch below the tunnel center line shows that the shock wave from the leading edge of the model is located behind $x = 8.25$ inches. The reflected wave from the wall is in the region from about $x = 9.5$ to 10 inches. Immediately behind this region is the wave reflected back from the model surface. Because the survey was made quite close to the model, the wave going to the model tends to overlap the wave reflected from the model. The pressure behind these two waves in the region behind about $x = 10.75$ inches is about the same as the pressure behind the incident leading-edge shock. The pressure in the region between the wall-reflected wave and the reflection of this wave from the model may be determined from the survey made 1 inch below the tunnel center line, in the region between about $x = 9.75$ and 10.4 inches. This pressure is also about the same as that behind the incident shock. Because the pressure behind the reflected wave is about the same as the pressure ahead of it, this is the condition at which the wall porosity and divergence combine to satisfy the free-air boundary condition at the wall behind the shock wave. However, a reflected wave has been found to remain in the flow, and this disturbance affects the pressures in a restricted region on the model. The question arises as to why, if the wall permits the required outflow, a disturbance still remains. The answer lies in the fact that the flow does not experience a single sharp turn but instead goes through several successive turns before the final constant pressure is reached behind the shock-boundary-layer intersection. A flow disturbance originates near the wall as a result of these turns. The nature of the disturbance, a compression followed by an expansion and then by a second compression, suggests that the boundary layer near the wall first thickens causing a compression, then thins, causing an expansion, and finally reaches equilibrium causing a final compression. This physical interpretation is supported by boundary-layer surveys which will be presented in the next section of this paper. An examination of the flow surveys shows that the expansion increases in strength as the divergence is increased. The compression-expansion-compression disturbance just described is not evident at a divergence of 10' (fig. 9(a)). Here the reflection seems to be almost entirely compression. Changing the divergence from 10' to 20' has a very large effect on the character of the reflected disturbance.

A comparison of these results with those for the deep slotted wall of reference 1 is of interest. The reflected disturbance for the deep slotted wall was similar to that for the perforated wall at the higher divergences in that it started with a compression followed by an expansion. Behind the expansion, however, the disturbances were not at all alike. With the perforated wall, the expansion was followed by a short compression region and then a region of essentially constant pressure

which extended back to the point where the disturbance that was reflected from the model was encountered. With the slotted wall, the expansion was followed by a long region of compression and there was no constant pressure region behind the compression. It was shown in reference 1 that this long compression must be connected with the flow behind the region of intersection of the incident shock and the wall. The outflow behind the shock apparently attains a final constant value in a much shorter distance for the perforated wall than for the deep slotted wall. This difference in the flow pattern behind the expansion for the two walls is thought to be due to a fundamental difference in the characteristics of the two types of wall. On the other hand, the similarity observed in the front part of the reflected disturbance for the two walls would seem to indicate that this part of the disturbance was connected with some factor which was common to the flow with both walls, in particular the boundary layer.

Boundary layer.- It was pointed out in reference 1 that the initial compression-expansion disturbance could result from a forward travel of the pressure field through either the boundary layer or the slots of the slotted wall. As mentioned previously, the perforated type of wall was selected for the present investigation in order to eliminate the latter possibility. Thus, when the compression-expansion disturbance was observed with the perforated wall, it appeared that the boundary layer must be responsible.

In order to obtain verification of this conclusion, concerning the primary influence of the wall boundary layer, total-pressure surveys of the boundary layer in the region near the shock wave were made with the walls set at 20' divergence (fig. 10(a)). These surveys show that the boundary layer is considerably thickened at a location ($x = 8.5$ inches) which is $1/2$ inch ahead of the shock-boundary-layer intersection. Between $x = 8$ and $x = 8.5$ inches, the boundary layer is growing at a rate several times higher than the rate of growth found upstream in the tunnel and it is this disproportionate thickening of the boundary layer which causes the first compression in the reflected disturbance of figure 9(c). The boundary-layer thickness begins to decrease somewhere upstream of $x = 8\frac{7}{8}$ inches although the shock does not intersect the boundary layer until it reaches $x = 9$ inches. This thinning of the boundary layer causes an expansion in the supersonic flow outside the boundary layer. It is evident from these results that the high-pressure field from behind the shock wave has traveled forward through the boundary layer under the shock wave and produced gross changes in the boundary-layer thickness upstream of the shock wave. These changes in the boundary-layer thickness are responsible for the complicated reflected disturbances found at the higher divergence angles.

Because of the change that was observed in the character of the reflected disturbance when the divergence was reduced to 10', boundary-layer surveys were also made at that wall setting (fig. 10(b)). These surveys indicated that the boundary layer ahead of the shock wave is essentially unaffected by the shock even at $x = \frac{87}{8}$ inches which is only 1/8 inch ahead of the shock-boundary-layer intersection. This is an entirely different result from that obtained at 20' divergence and is sufficient explanation for the change in the character of the reflected disturbance.

It is encouraging to find that it is experimentally possible to prevent a shock wave from influencing the boundary layer far upstream of the shock, but it is also important to note that the prevention required an extremely thin boundary layer ($\delta^* \approx 0.008$ inch) in the present case.

Schlieren photographs.— Schlieren photographs were made with a horizontal knife edge at wall divergence angles of 10', 20', and 30' (fig. 11). The pressure data were obtained in the region between the model and the bottom wall. These photographs serve to confirm the flow description which has been given. The increase in boundary-layer thickness with increasing wall divergence is clearly visible, as is the reflected disturbance at 20' divergence (dark compression, light expansion, and dark compression in the lower part of the picture). The thinning of the boundary layer ahead of the shock-boundary-layer intersection is not visible in the pictures, perhaps because of the thickened boundary layer in the corners of the tunnel. At 10' divergence, the photograph shows a very weak compression-expansion-compression disturbance which was apparently too small to be detected by the static-pressure probe. The weak disturbance observed to originate about 3/4 inch downstream of the reflection is not due to the model. This disturbance can be observed in the tunnel-empty condition (see fig. 5(a)) originating at the lower wall below the rear model-support hole.

The angle of attack is such that the shock wave above the model is somewhat stronger than that below the model. It appears that the character of the reflection is influenced by the shock strength. For instance, the reflection in the upper half of the flow field at a wall divergence angle of 20' appears to be quite different from that in the lower half of the field. The upper half of the flow field for 10' divergence is especially interesting because the stronger shock wave in this case seems to have been essentially canceled at the wall. It is unsafe, however, to draw any conclusions with regard to interference from schlieren pictures in the absence of pressure data. This picture introduces the possibility that the wall behavior in attenuating shock waves, for a given open ratio and boundary layer, may well be influenced by the strength of the incident shock. This variable was not investigated, however, in this series of tests.

Boundary-Layer Equations

It is of interest to derive the equations which describe the behavior of the boundary layer on a porous wall to which suction is applied, and from these equations to determine the relationships between the rate of growth of the boundary layer, the suction mass flow, and the porous-wall friction coefficient.

Momentum equation.- Following the procedure of references 3 and 4, the compressible-flow momentum equation for a porous wall with suction may be derived readily as follows:

$$\frac{d\theta}{dx} + \theta \left(\frac{H+2}{U} \right) \frac{dU}{dx} + \frac{\theta}{\rho_\delta} \frac{d\rho_\delta}{dx} = \frac{C_f}{2} - \frac{\rho_0 v_0}{\rho_\delta U} \quad (1)$$

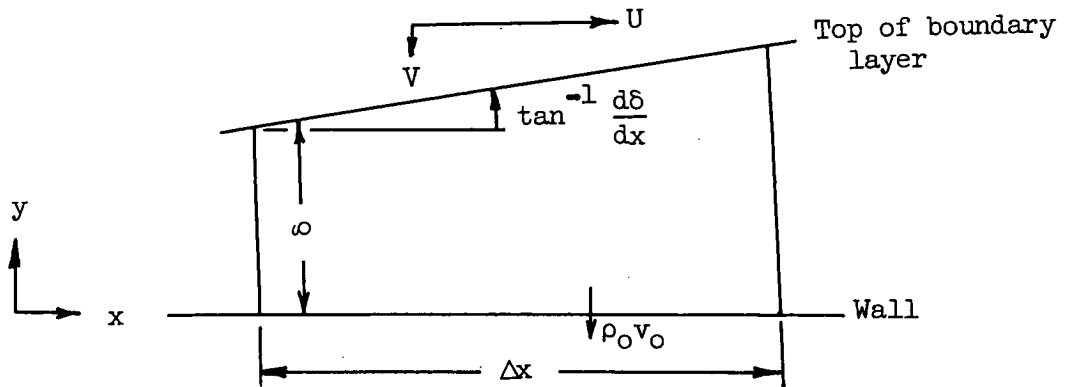
where

- θ boundary-layer momentum thickness
- H boundary-layer shape parameter
- U free-stream velocity
- ρ_δ free-stream density
- C_f effective wall friction coefficient
- $\rho_0 v_0$ suction mass flow per unit porous wall area

In the derivation of the boundary-layer momentum equation without suction the air at the surface of the wall is assumed to have zero momentum. In the case of the perforated wall the momentum at the surface of the wall is not strictly zero inasmuch as the air at the holes will, in general, possess some momentum. This momentum is lost, however, either in passing through the holes or in the plenum chamber outside the wall. For this reason the momentum entering the wall has been treated as a loss due to the wall, and is included in the effective friction coefficient. This has been accomplished in the derivation of equation (1) simply by assigning zero momentum to the air removed by suction ($\rho_0 v_0$).

Continuity equation.- Because of the presence of suction, the free-stream flow just outside the boundary layer will, in general, have a small component in a direction which is normal to the wall. It is often necessary to relate this component to the suction flow. This may be accomplished by means of the continuity equation.

Consider the following sketch of a growing boundary layer adjacent to a porous wall:



The inflow at the top of the boundary layer is

$$\rho_{\delta} \left(U \frac{d\delta}{dx} + v \right) \Delta x$$

It is assumed here that the normal component of the velocity is sufficiently small so that the parallel component can be treated as equal to the free-stream velocity U . This is certainly justified in the case of the small outflow angles encountered in the present investigation.

The inflow at the left is

$$\int_0^{\delta} \rho u \, dy$$

The outflow at the right is

$$\int_0^{\delta} \rho u \, dy + \frac{d}{dx} \int_0^{\delta} \rho u \, dy \, \Delta x$$

The outflow at the bottom is

$$\rho_0 v_0 \, \Delta x$$

Combining these flows gives the continuity equation

$$\rho_0 v_0 + \frac{d}{dx} \int_0^{\delta} \rho u \, dy = \rho_{\delta} \left(U \frac{d\delta}{dx} + V \right)$$

Alternatively, the second term can be written as

$$\frac{d}{dx} \int_0^{\delta} \rho u \, dy = \rho_{\delta} U \frac{d\delta}{dx} - \rho_{\delta} U \frac{d\delta^*}{dx} + (\delta - \delta^*) \frac{d}{dx} (\rho_{\delta} U)$$

The continuity equation is then

$$\rho_0 v_0 = \rho_{\delta} V + \rho_{\delta} U \frac{d\delta^*}{dx} - (\delta - \delta^*) \frac{d}{dx} (\rho_{\delta} U)$$

or

$$\frac{\rho_0 v_0}{\rho_{\delta} U} = \frac{V}{U} + \frac{d\delta^*}{dx} - (\delta - \delta^*) \frac{\frac{d}{dx} (\rho_{\delta} U)}{\rho_{\delta} U} \quad (2)$$

Boundary-layer equations for uniform flow in a wind tunnel.— The equations simplify considerably for the case of uniform flow. In this case

$$\frac{dU}{dx} = \frac{d\rho_{\delta}}{dx} = 0$$

and the momentum equation becomes simply

$$\frac{d\theta}{dx} = \frac{C_f}{2} - \frac{\rho_0 v_0}{\rho_{\delta} U} \quad (3)$$

The continuity equation reduces to

$$\frac{\rho_0 v_0}{\rho_{\delta} U} = \frac{V}{U} + \frac{d\delta^*}{dx}$$

In the case of uniform flow in a wind tunnel, the term $\frac{V}{U}$ is equal to the negative tangent of the wall divergence angle γ . Thus

$$\frac{\rho_0 v_0}{\rho_{\delta} U} = -\tan \gamma + \frac{d\delta^*}{dx} \quad (4)$$

Equation (3) makes it possible to compute the wall friction coefficient if suction flow and boundary-layer measurements are available. A further modification of equation (3) is possible. By definition, the boundary-layer shape parameter is

$$H = \frac{\delta^*}{\theta}$$

so

$$\frac{d\theta}{dx} = \frac{1}{H} \frac{d\delta^*}{dx} - \frac{\delta^*}{H^2} \frac{dH}{dx}$$

The last term is normally quite negligible for uniform flow, so the momentum equation becomes

$$\frac{1}{H} \frac{d\delta^*}{dx} \approx \frac{C_f}{2} - \frac{\rho_0 v_0}{\rho_\delta U} \quad (5)$$

Equations (4) and (5) show the interdependence for uniform flow in the tunnel between the suction flow, the rate of increase of the boundary-layer displacement thickness, and the wall friction coefficient. If any one of these three quantities is known, the other two can be determined from these equations. It is assumed here that the wall divergence angle and the wall boundary-layer shape parameter are known.

Use of continuity equation to check accuracy of boundary-layer measurements.— Because the continuity equation relates the boundary-layer growth to the suction flow, it can be used as a check on the accuracy of the boundary-layer measurements if the suction flow has also been measured. In the case of a complete wind tunnel, the continuity equation must be applied to all four walls. In the case of a tunnel with top and bottom walls porous and of width w , and with parallel side walls solid and of height h , the continuity equation is

$$\frac{\Delta m}{m} = \frac{2l}{h} \left(-\tan \gamma + \frac{d\delta_p^*}{dx} \right) + \frac{2l}{w} \frac{d\delta_s^*}{dx} \quad (6)$$

where

- Δm suction mass flow
- m mass flow entering porous test section
- l length of porous test section

- γ porous-wall divergence angle
- δ^*_p boundary-layer displacement thickness on porous wall
- δ^*_s boundary-layer displacement thickness on solid side wall

The boundary-layer measurements obtained in this investigation at $M = 0.98$ have been inserted in this equation in order to compute the suction mass-flow ratio. In addition to the data which have been presented so far, it was necessary to measure also the side-wall boundary layer in order to make this computation. Side-wall velocity profiles were measured at stations 3.5 and 9.0 at a Mach number of 0.98, using a total-pressure probe which was inserted through the holes in the side walls. The value of $\frac{d\delta^*_s}{dx}$ determined from these measurements is 0.00205. Because of the reduced spacing between survey stations, and because the transition from laminar to turbulent boundary-layer flow on the side walls occurs within the test section, this value is regarded as somewhat less accurate than the values of $\frac{d\delta^*}{dx}$ for the perforated wall which were presented in figure 7.

The computed suction mass-flow ratios are compared in figure 12 with measured suction ratios as determined with the calibrated orifice plate. The agreement is such that the accuracy of the boundary-layer measurements is regarded as satisfactory. The most pronounced disagreement occurs at a wall divergence of 15° , in which case the pressure differential across the orifice plate was less than 2 inches of kerosene. Because of this low differential, and the correspondingly low orifice Reynolds number, the suction measurements are less accurate for this condition than with the walls parallel or converged.

Use of momentum equation to compute effective friction coefficients.- A knowledge of the effective friction coefficients for perforated walls would be very useful in the design of a perforated-wall wind tunnel. Furthermore, it is of some general interest to know how the friction coefficients for perforated walls compare in magnitude with those for solid walls. Equation (3) has therefore been used to compute friction coefficients for the perforated walls used in this investigation from the measured values of suction flow and $\frac{d\theta}{dx}$. The measured values of $\frac{d\theta}{dx}$ are, of course, average values over the length of the wall so the computed friction coefficients are also average values. These friction coefficients have been plotted against the boundary-layer Reynolds number R_θ in figure 13. Because of the large increase in Reynolds number between the front and rear of the test section, a crosshatched region

is shown in figure 13 which extends from values of R_θ at $x = 1.0$ inch to R_θ at $x = 10.5$ inches. A comparison with the smooth-wall friction coefficients as given by Squire and Young (ref. 5) shows that the effective perforated-wall friction coefficients for thin boundary layers (low R_θ) are much greater than the corresponding smooth-wall friction coefficients.

The fact that the effective friction coefficient is plotted against R_θ is not meant to exclude the possibility that it may also be a function of other parameters. In this investigation, for example, the side walls were parallel. If these walls were diverged the suction mass flow would be reduced. The result would be a lower C_f and a higher R_θ on the perforated walls, but it is possible that the plot of C_f against R_θ with the side walls diverged would be different than with the side walls parallel.

CONCLUDING REMARKS

The results of an investigation of a two-dimensional transonic test section incorporating two 17-percent-open perforated walls are summarized in the following remarks:

1. A test section flow of acceptable uniformity was obtained through the Mach number range tested (0.8 to 1.3) with perforated walls of constant open ratio. Wall divergence was used to eliminate a positive velocity gradient at the higher Mach numbers.
2. Under the test conditions with the walls diverged at an angle of 25', the wall divergence and the porosity characteristics of the 17-percent-open perforated wall combined to allow the flow near the wall to turn to the correct (interference-free) direction after passing through the region near the shock wave; but a disturbance, which consisted of a compression followed by an expansion and then a second compression, was reflected from the region of turning. This disturbance was weaker and affected a smaller portion of the model than the disturbance reflected from a multislot-type wall previously investigated.
3. The compression-expansion-compression disturbance, which was present at all divergence angles in excess of 10', was found to be caused by interaction between the shock wave and boundary layer.
4. It was possible to prevent the shock from thickening the boundary layer ahead of the shock by reducing the wall divergence to 10'. In this case, the displacement thickness of the boundary layer just ahead of the

shock was only 0.008 inch. However, the wall was not sufficiently open to prevent a reflected compression at this divergence angle.

5. Turbulent-type velocity profiles were found in the boundary layer adjacent to the perforated walls. With the tunnel empty, increasing the perforated wall divergence angle from $-15'$ to $30'$ increased the rate of growth of the boundary-layer displacement thickness from 0.00048 to 0.00570 inch per inch at a Mach number of 0.98.

6. Disturbances of unknown magnitude were found to emanate from the individual holes in the perforated walls. The schlieren photographs showed that with the walls parallel these disturbances could be traced across the tunnel. With the walls diverged $30'$ these disturbances became less prominent as the boundary layer thickened.

7. Suction mass flows computed by using the boundary-layer data in the boundary-layer continuity equation were found to be in good agreement with the measured suction mass flows at a Mach number of 0.98.

Langley Aeronautical Laboratory,
National Advisory Committee for Aeronautics,
Langley Field, Va., February 1, 1954.

REFERENCES

1. Sellers, Thomas B., Davis, Don D., and Stokes, George M.: An Experimental Investigation of the Transonic-Flow-Generation and Shock-Wave-Reflection Characteristics of a Two-Dimensional Wind Tunnel With 24-Percent-Open, Deep, Multislotted Walls. NACA RM L53J28, 1953.
2. Stokes, George M., Davis, Don D., Jr., and Sellers, Thomas B.: An Experimental Study of the Porosity Characteristics of Perforated Materials in Normal and Parallel Flow. NACA TN 3085, 1954.
3. Tetervin, Neal: Approximate Formulas for the Computation of Turbulent Boundary-Layer Momentum Thicknesses in Compressible Flows. NACA ACR L6A22, 1946.
4. Schlichting H.: An Approximate Method for Calculation of the Laminar Boundary Layer With Suction for Bodies of Arbitrary Shape. NACA TM 1216, 1949.
5. Squire, H. B., and Young, A. D.: The Calculation of the Profile Drag of Aerofoils. R. & M. No. 1838, British A.R.C., 1938.

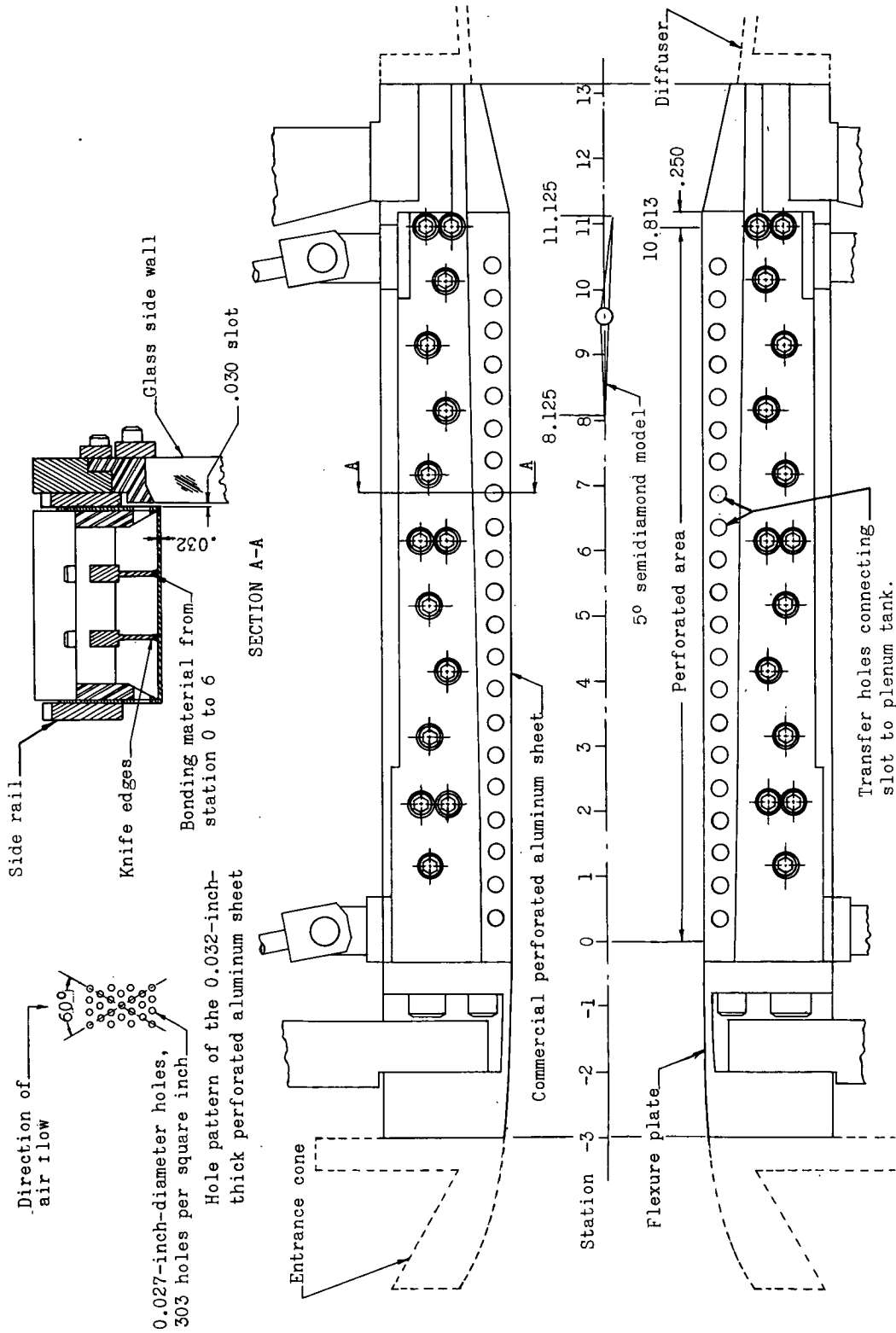
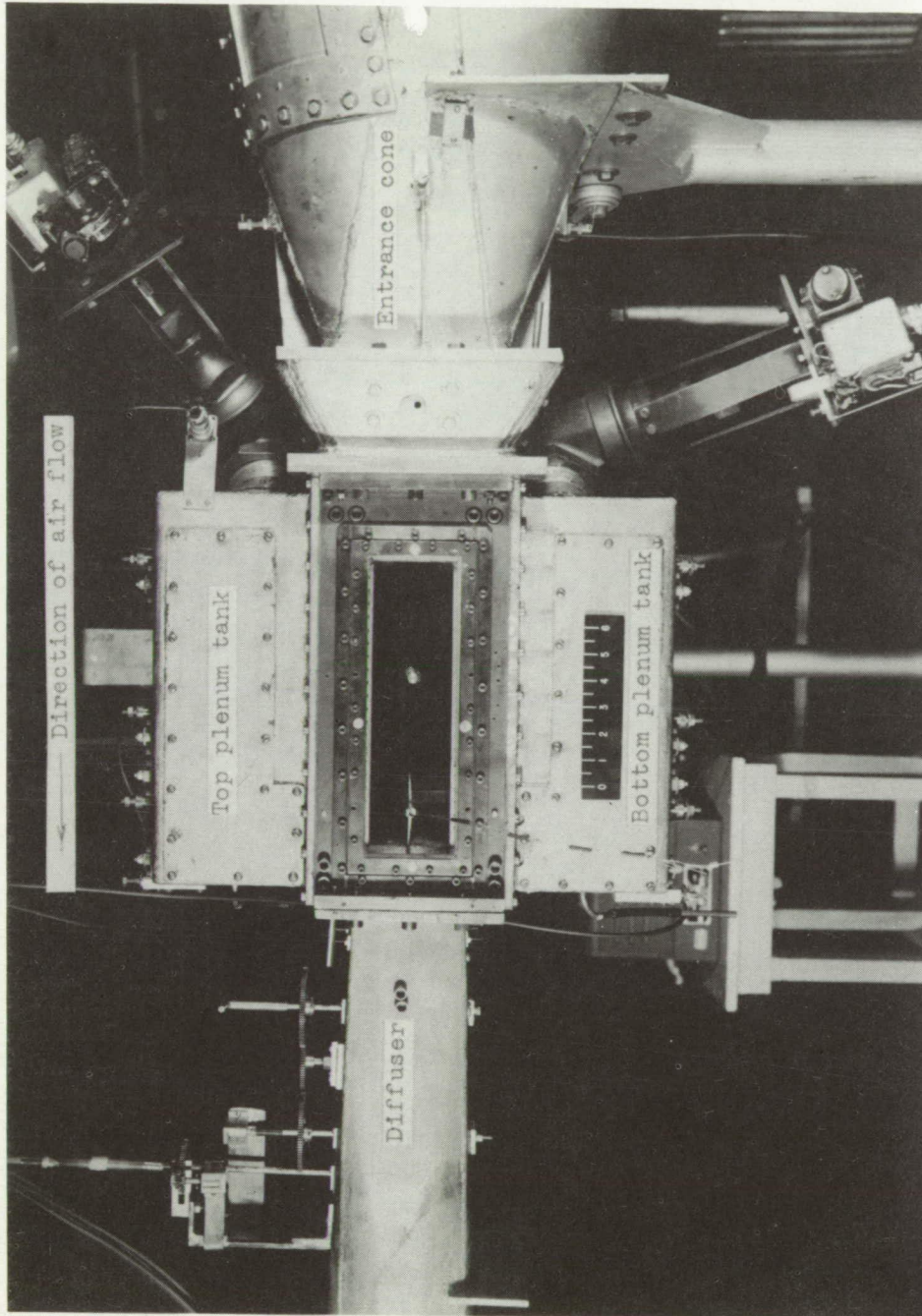


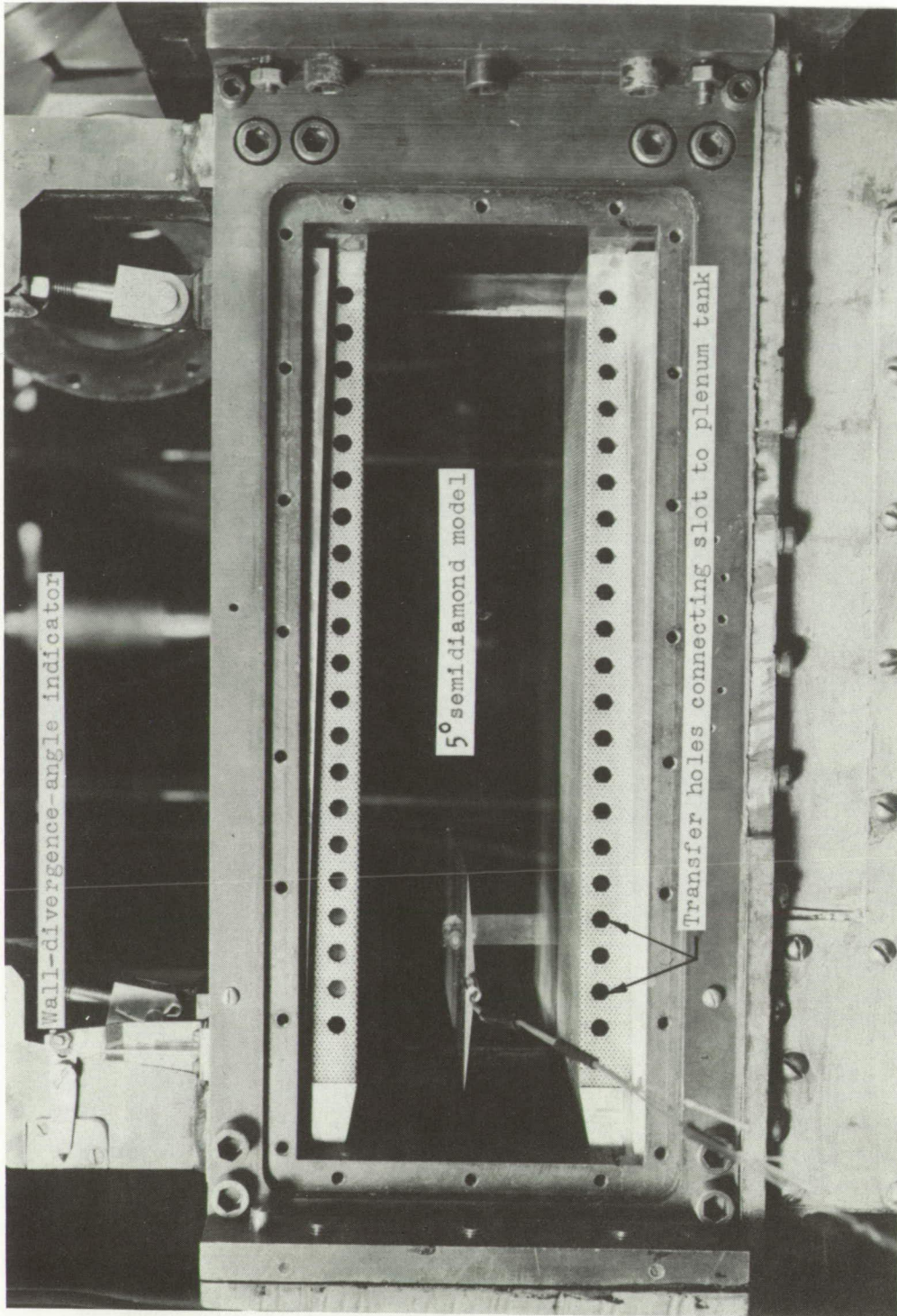
Figure 1.- Details and dimensions of the 17-percent-open perforated-sheet test section. One side wall removed. All dimensions are in inches.



L-79399.1

(a) General view of the removable test section mounted in the tunnel circuit.
Model installed.

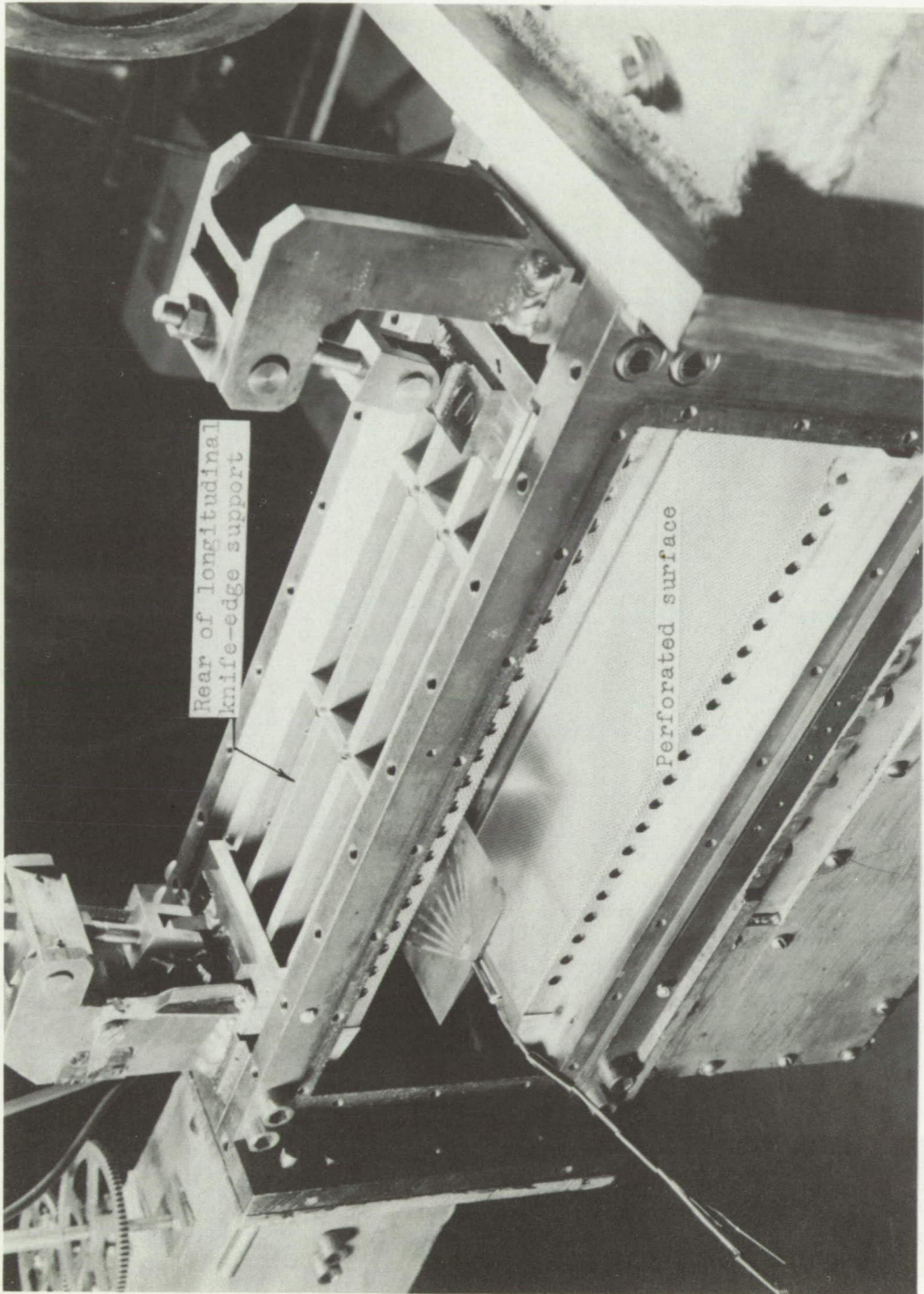
Figure 2.- Photographs of the transonic-flow-apparatus removable test section fitted with 17-percent-open, 0.027-inch hole-diameter, perforated-sheet walls. Model mounted in the test section.



L-79401.1

(b) Glass side wall removed. Model installed.

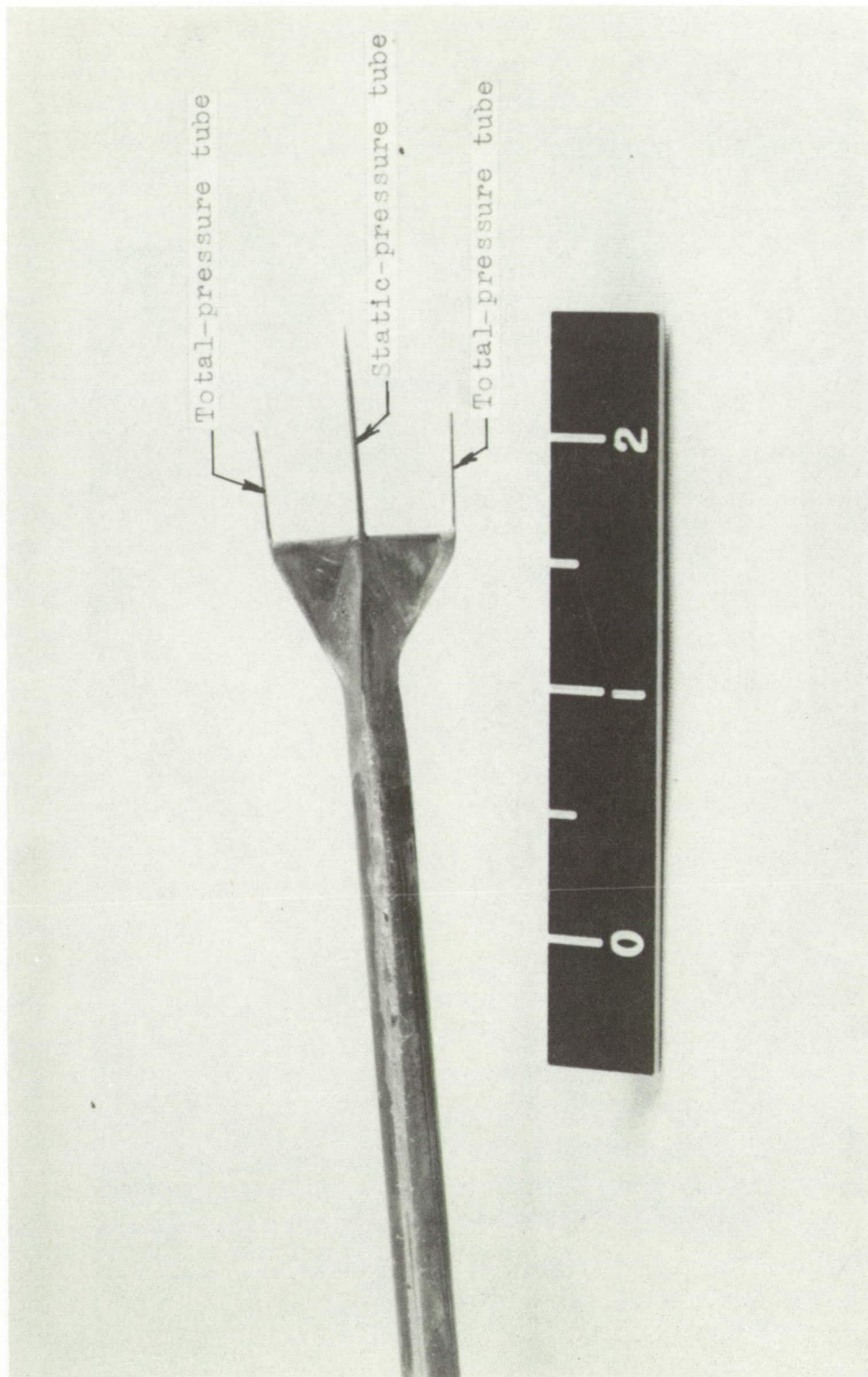
Figure 2.- Continued.



L-79400.1

(c) Details of knife-edge support system.

Figure 2.- Concluded.



L-81652.1

Figure 3.- Photograph of the boundary-layer probe.

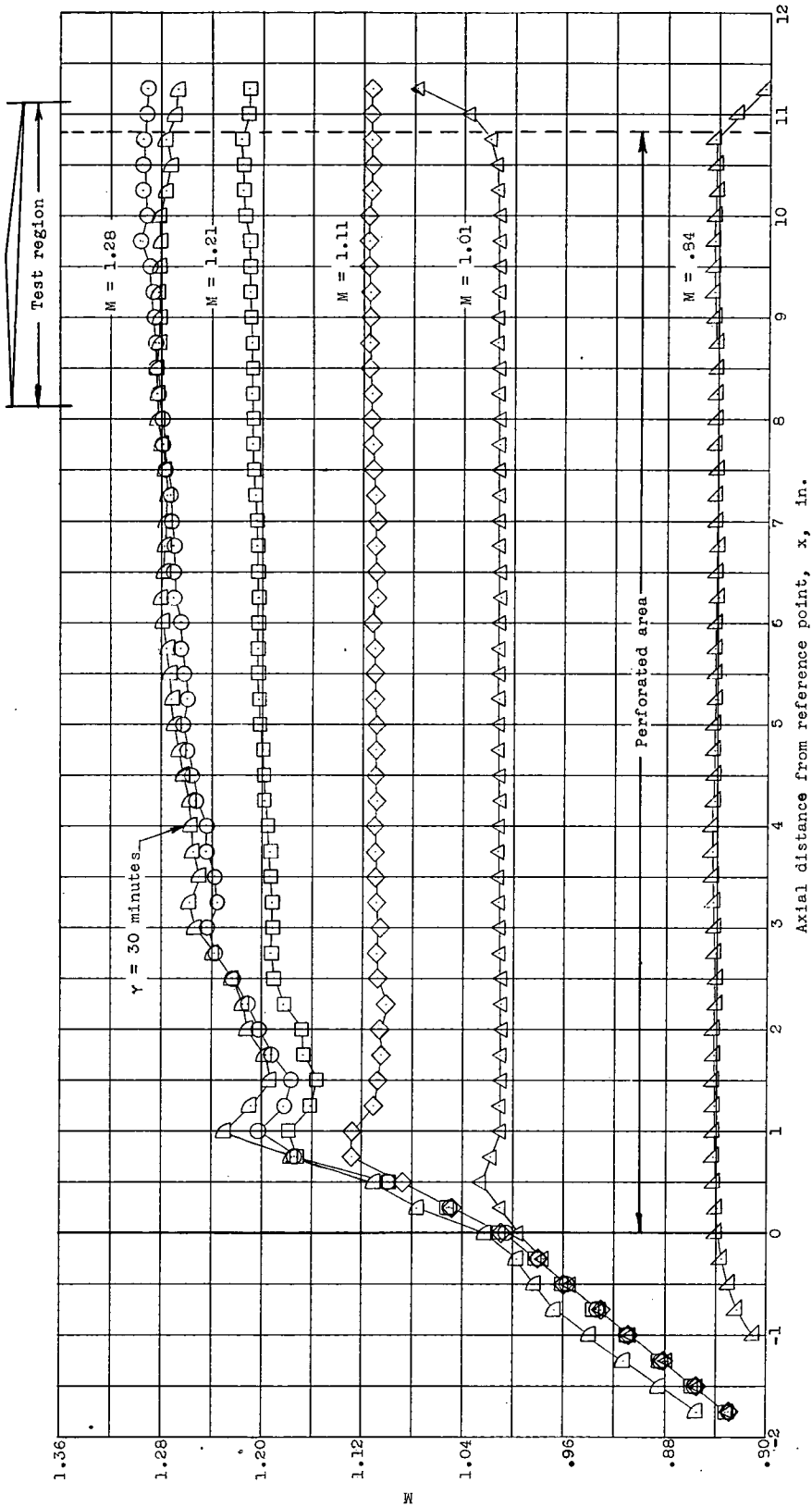
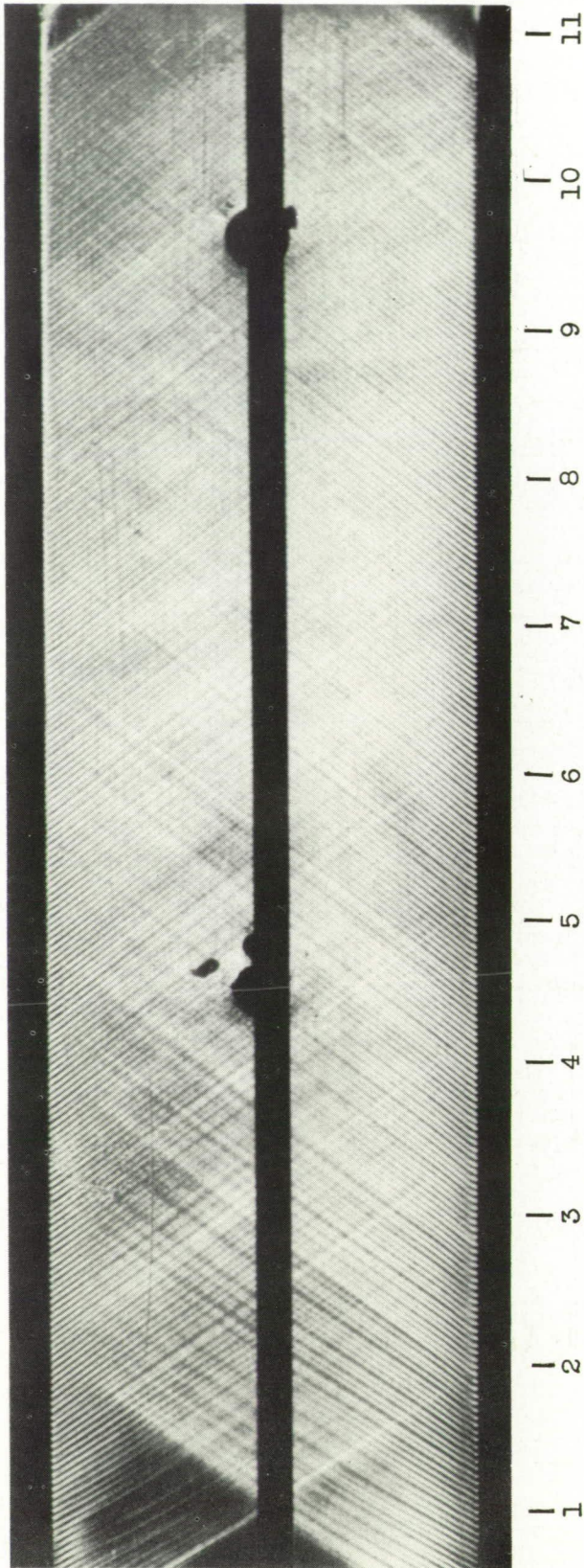


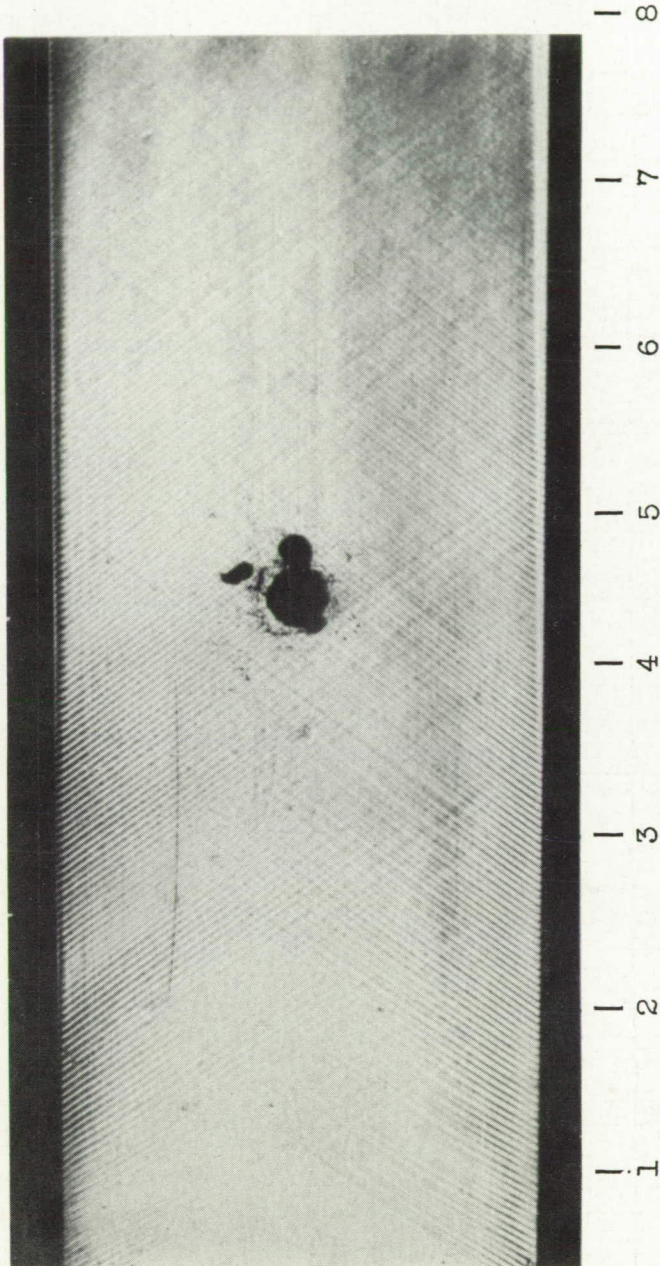
Figure 4.- Center-line Mach number distribution over a Mach number range. $\gamma = 0'$ except where noted otherwise.



L-83286

(a) $\gamma = 0'$. Knife edge vertical.

Figure 5.- Schlieren photographs of the flow in the 17-percent-open perforated-wall test section.
 $M = 1.28$.



Axial distance from reference point, x, in.

L-83287

(b) $\gamma = 30'$. Knife edge horizontal.

Figure 5.- Concluded.

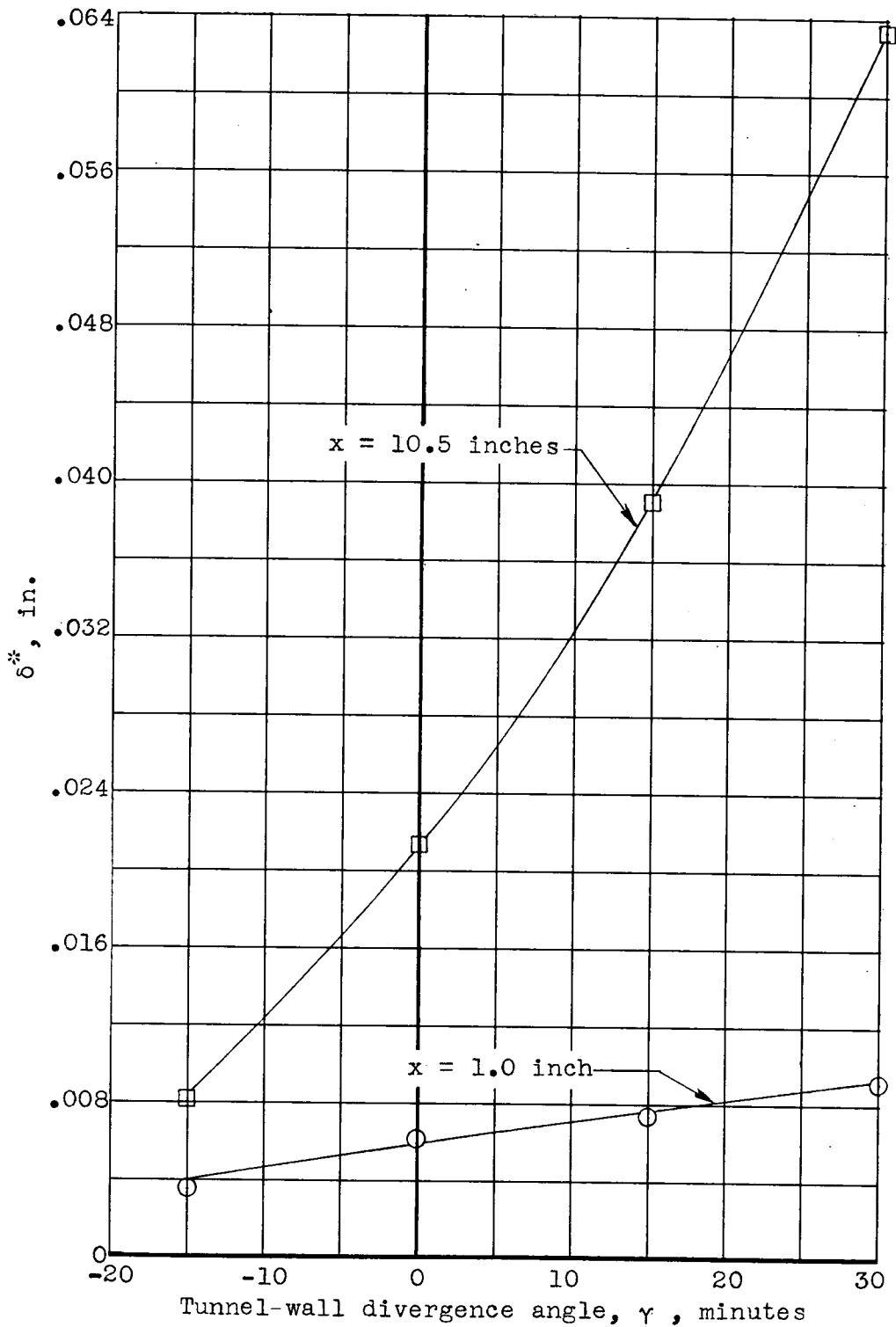


Figure 6.- Effect of increasing the wall divergence angle on the perforated-wall boundary-layer displacement thickness at two longitudinal locations. $M = 0.98$.

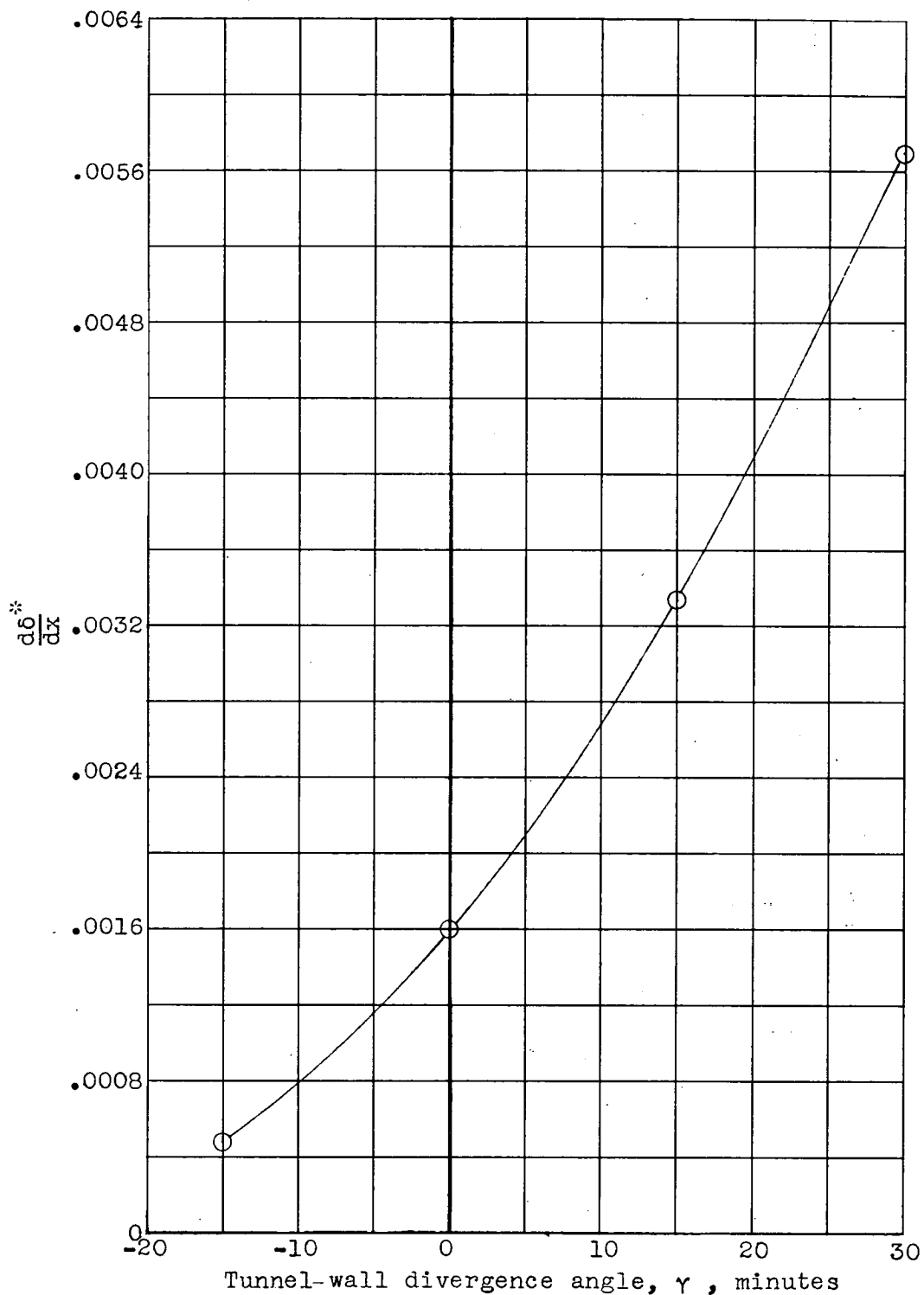


Figure 7.- Effect of increasing the wall divergence angle on the rate of increase in the perforated-wall boundary-layer displacement thickness. $M = 0.98$.

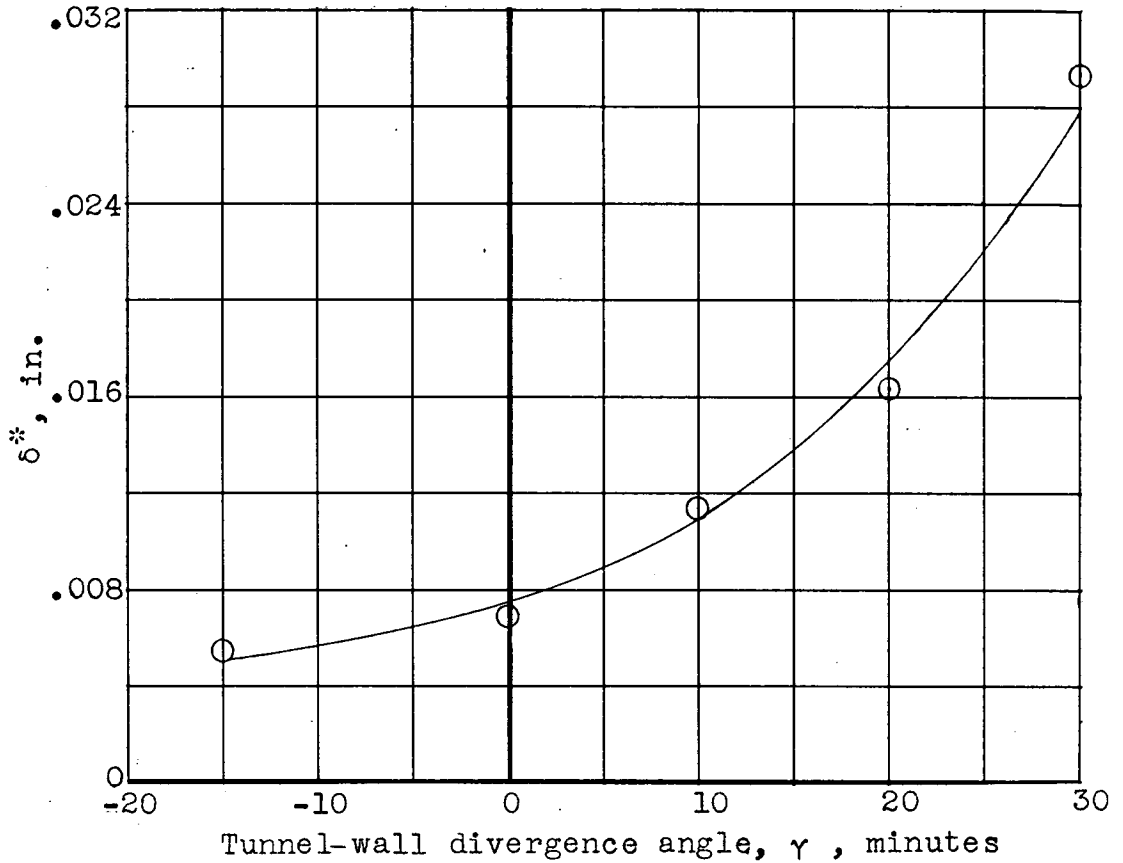
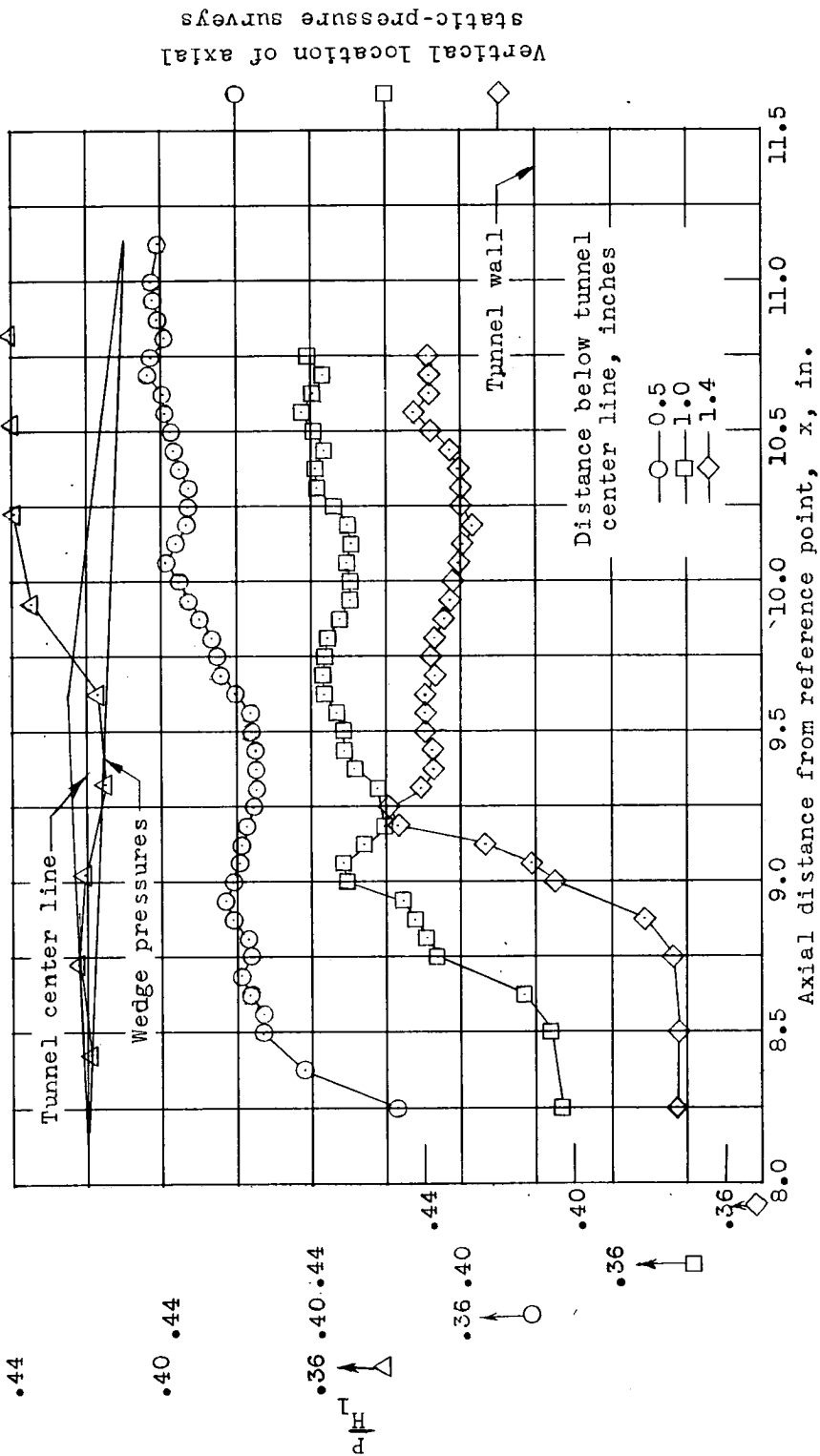


Figure 8.- Effect of increasing the wall divergence angle on the perforated-wall boundary-layer displacement thickness at $x = 10.5$ inches. $M = 1.28$.



(a) $\gamma = 10'$; $\delta^* \approx 0.007$ inch at $x = 8.0$ inches; $\delta^* \approx 0.008$ inch at $x = 8.5$ inches.

Figure 9.- Wedge surface pressures and longitudinal static-pressure surveys in the flow field adjacent to the wedge model mounted in the 17-percent-open perforated-sheet test section for several wall divergence angles and perforated-wall boundary-layer displacement thicknesses. Free-stream $\frac{P}{P_\infty}$ corresponding to a Mach number of 1.28; $\Delta M = 0.09$.

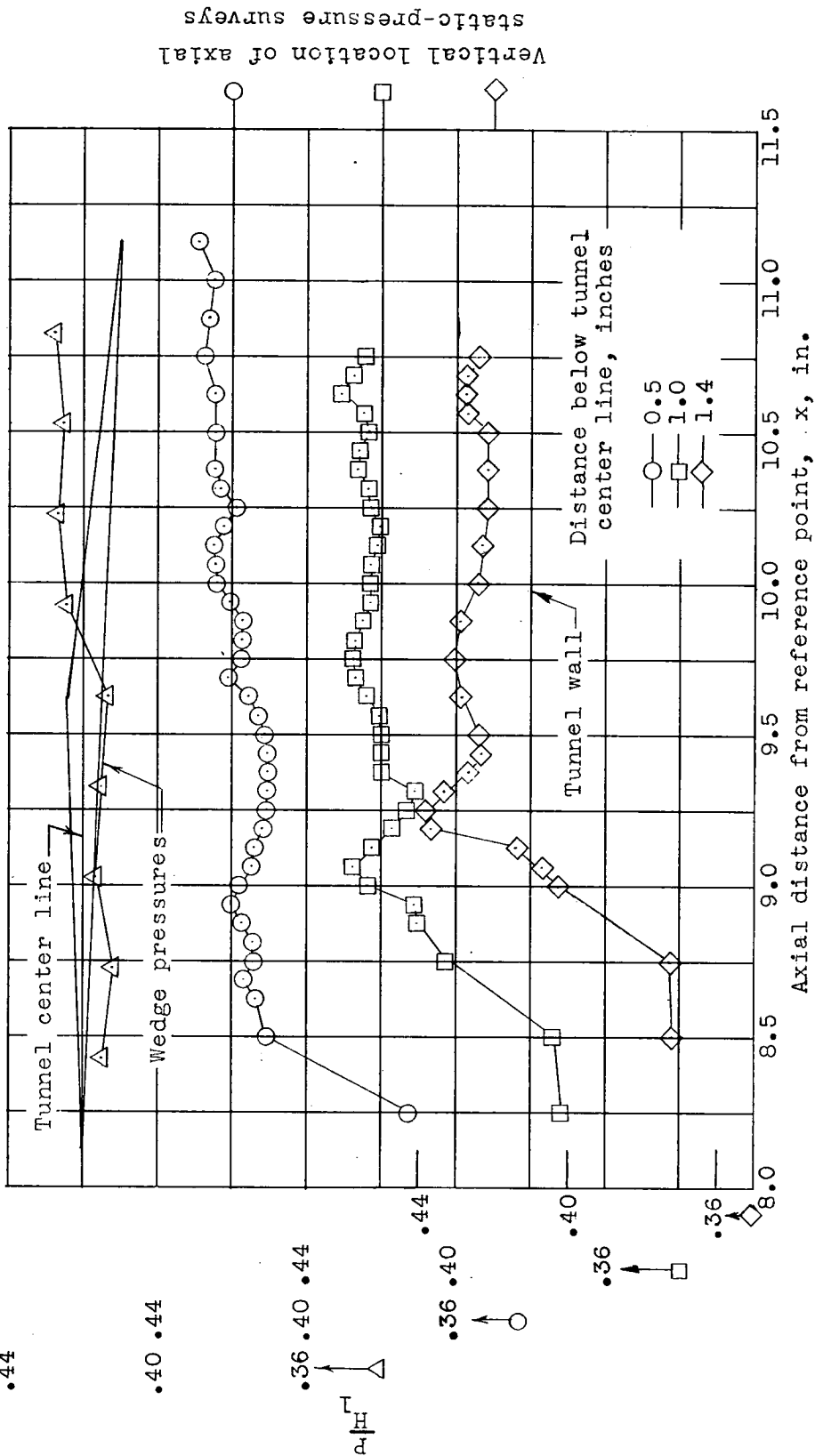
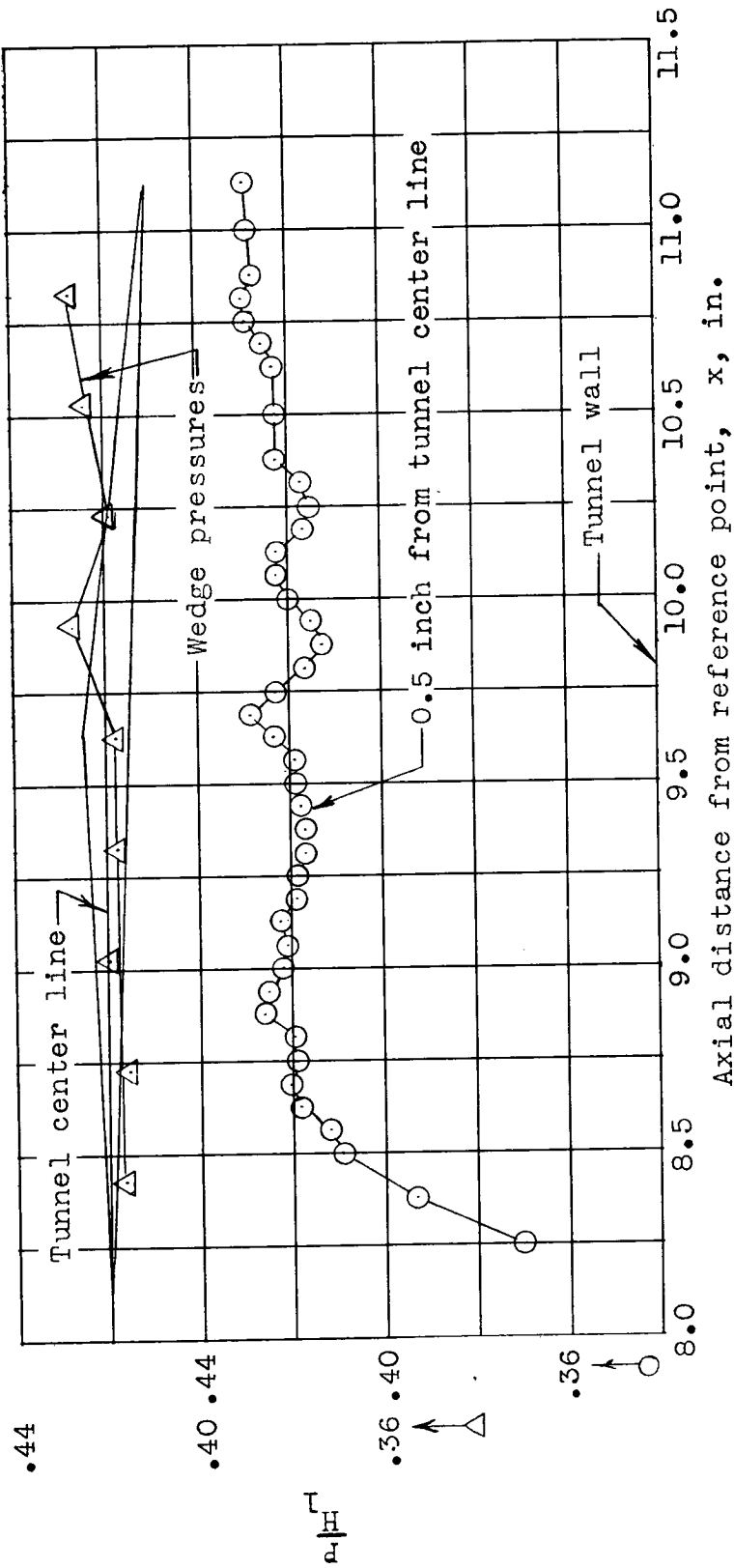
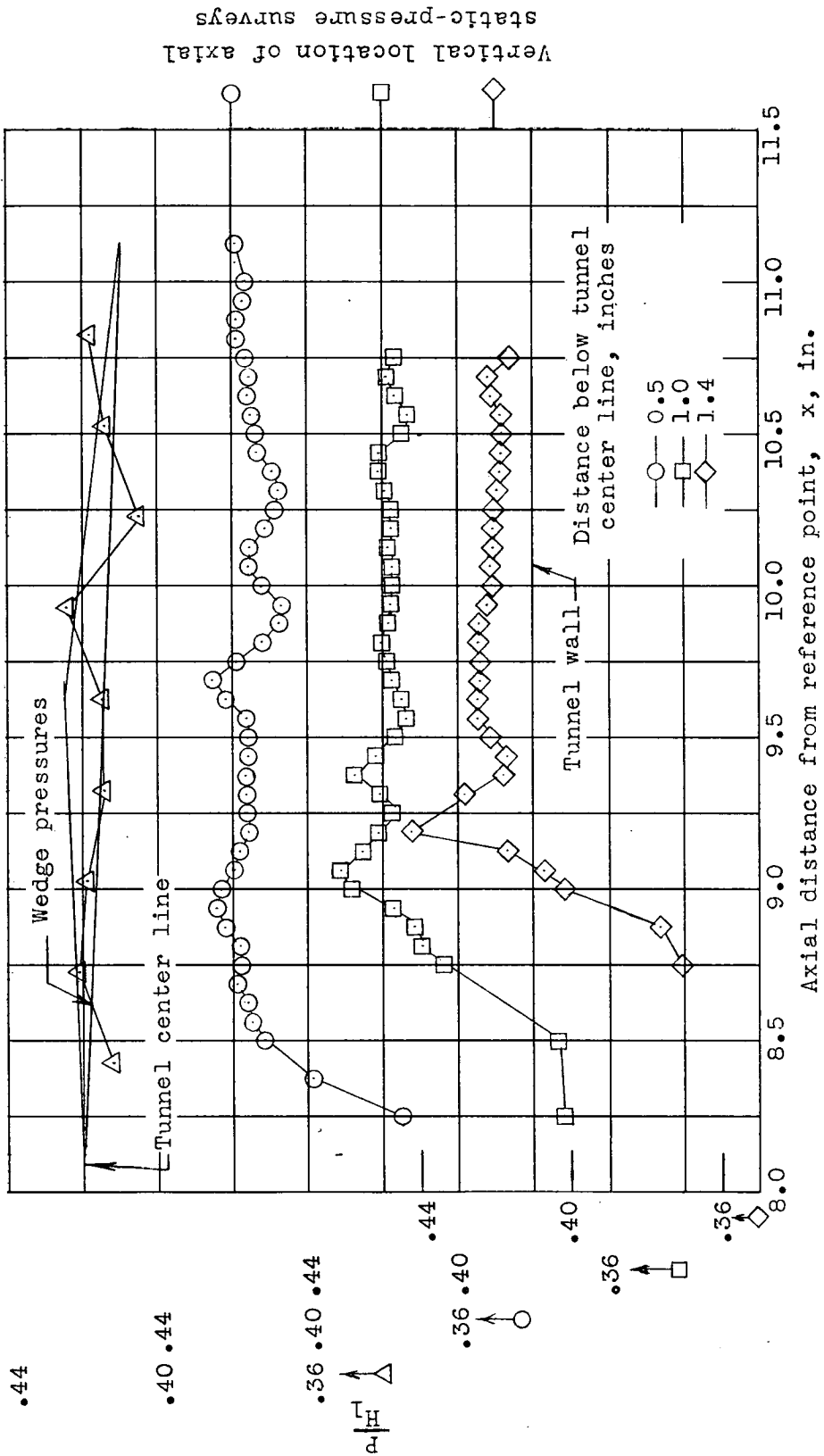


Figure 9.- Continued.



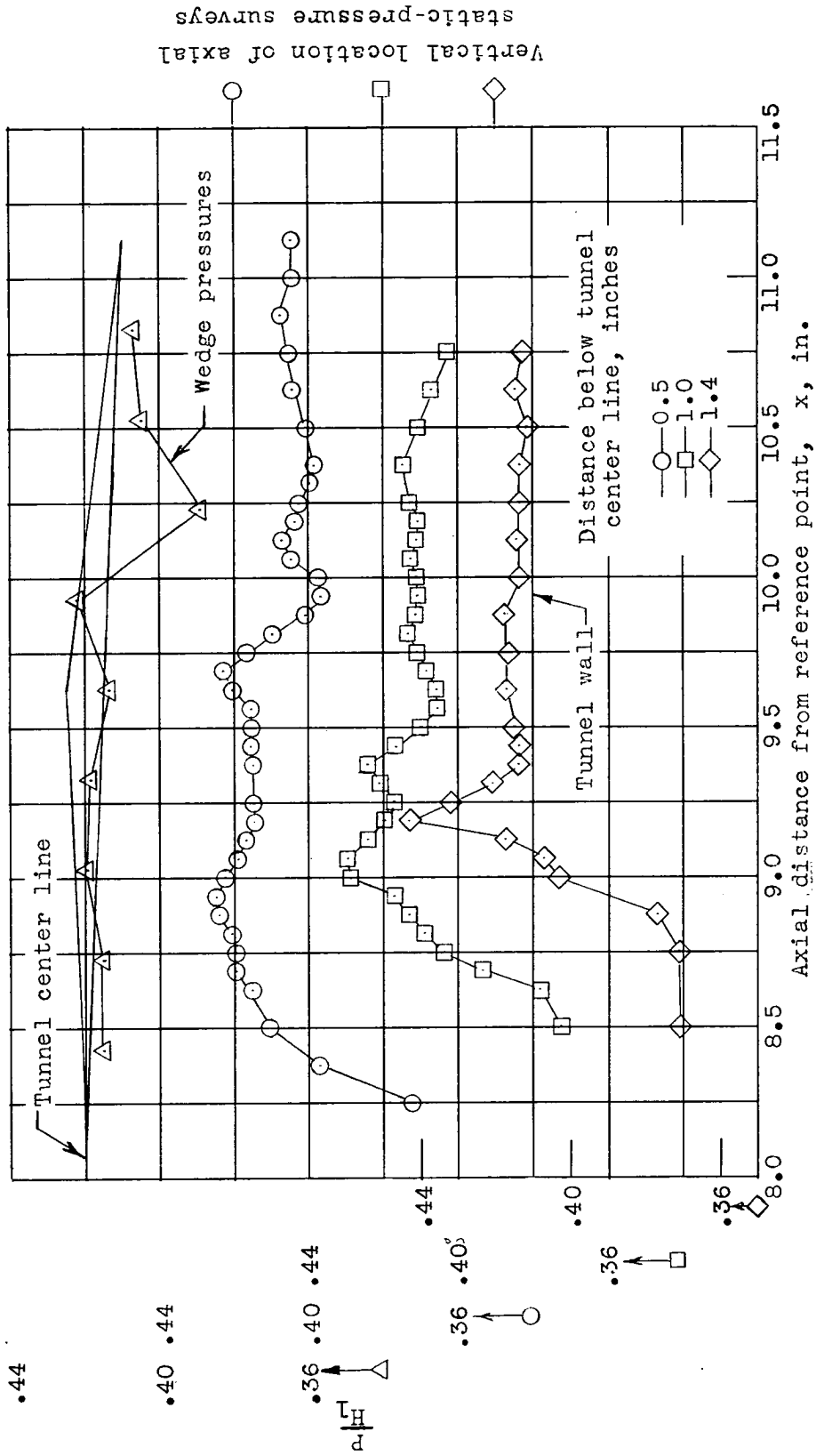
(c) $\gamma = 20^\circ$; $\delta^* \approx 0.010$ inch at $x = 8.0$ inches; $\delta^* \approx 0.017$ inch at $x = 8.5$ inches.

Figure 9.- Continued.



(a) $\gamma = 25'$.

Figure 9.- Continued.



(e) $\gamma = 30'$.

Figure 9.- Concluded.

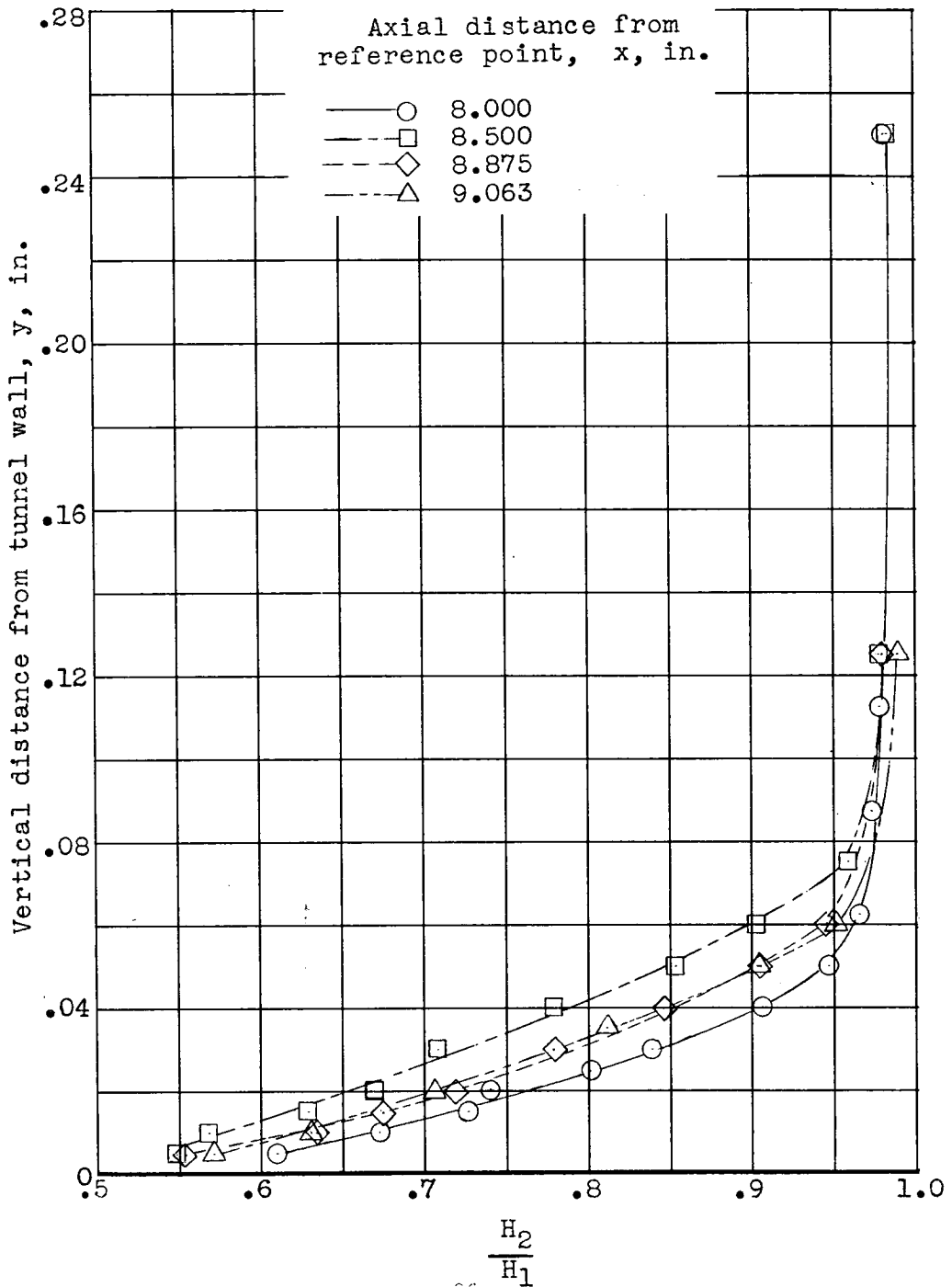
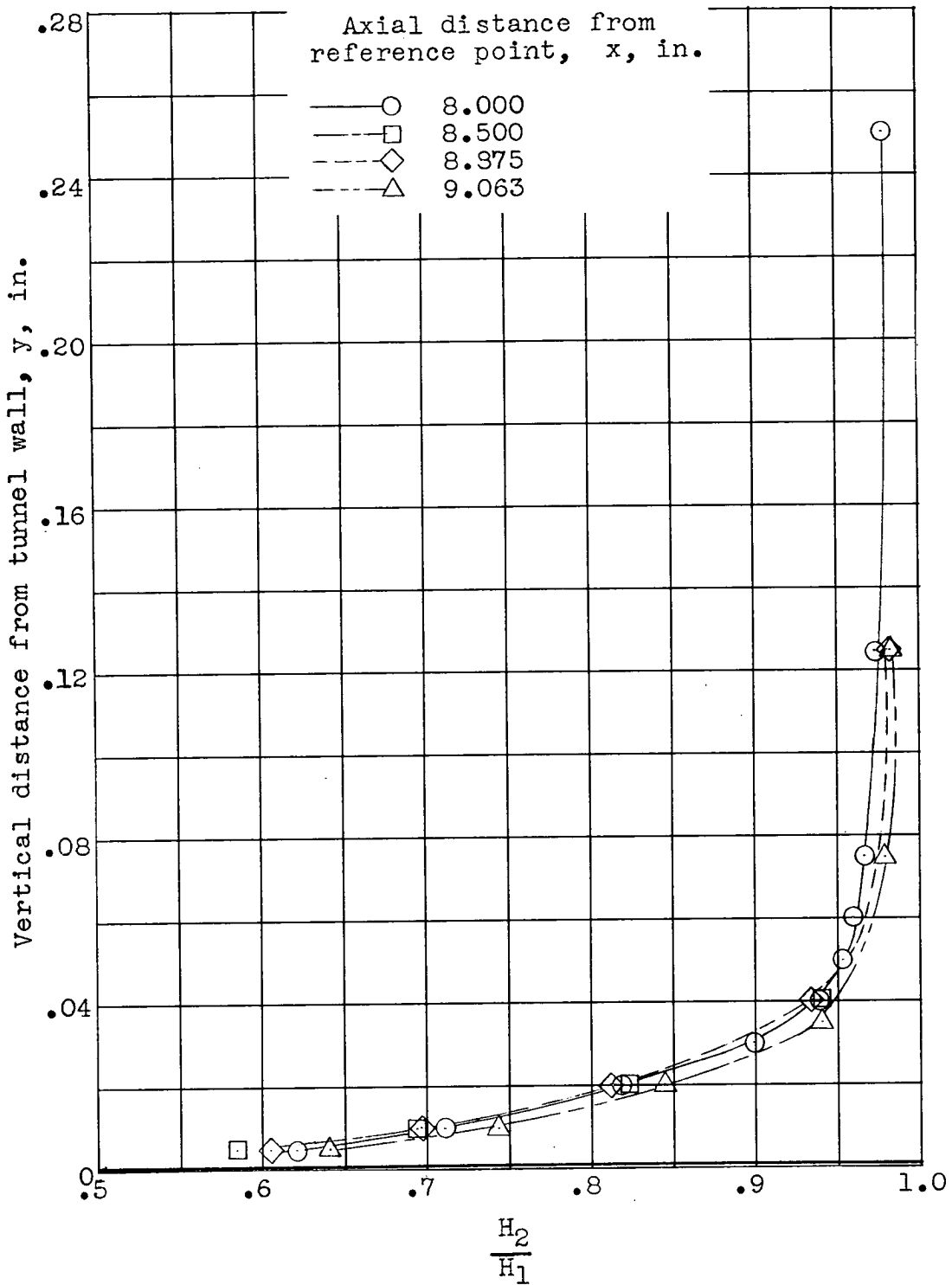
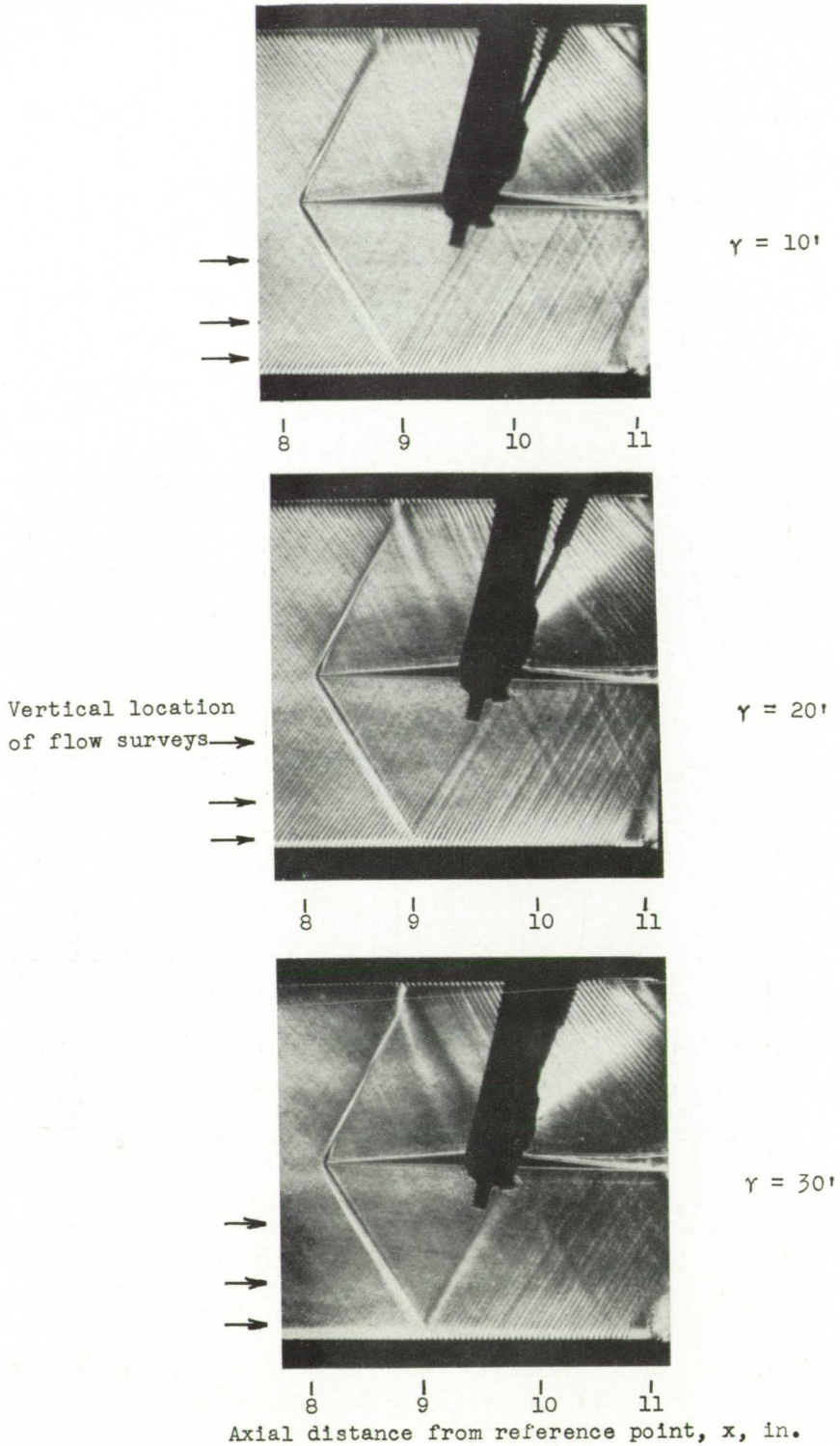
(a) $\gamma = 20'$.

Figure 10.- Boundary-layer total-pressure measurements at several horizontal stations near the incident shock-wave boundary-layer intersection ($x = 9.00$ inches) for two tunnel-wall divergence angles. Model in tunnel; $\Delta M = 0.09$; $M = 1.28$.



(b) $\gamma = 10'$.

Figure 10.- Concluded.



L-83288

Figure 11.- Schlieren photographs of the flow field adjacent to a 5° semi-diamond model mounted in a 17-percent-open perforated-wall wind tunnel with the walls at three divergence angles. Free-stream $M = 1.28$; $\Delta M = 0.09$.

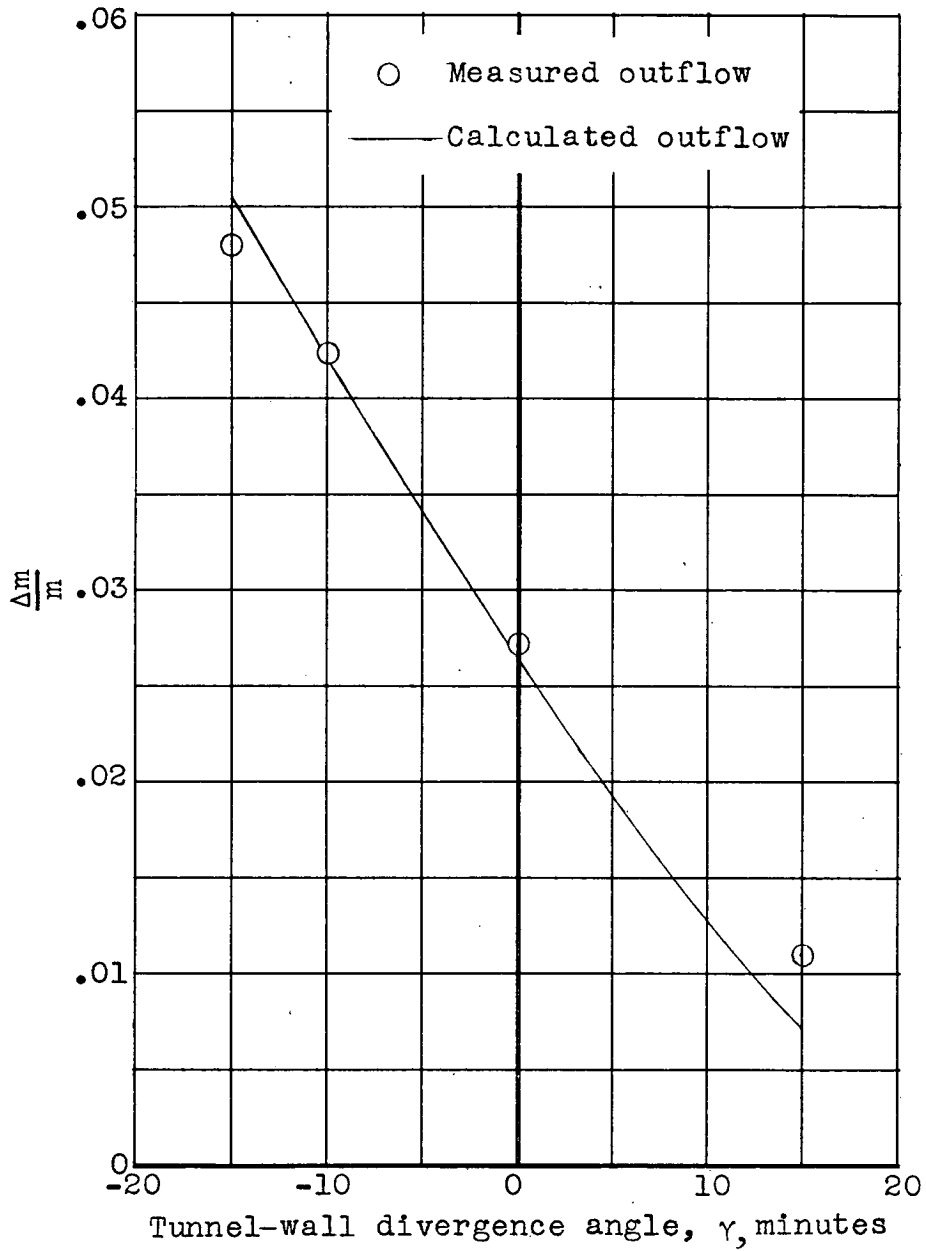


Figure 12.- Effect of increasing the wall divergence angle on the suction mass flow. $M = 0.98$.

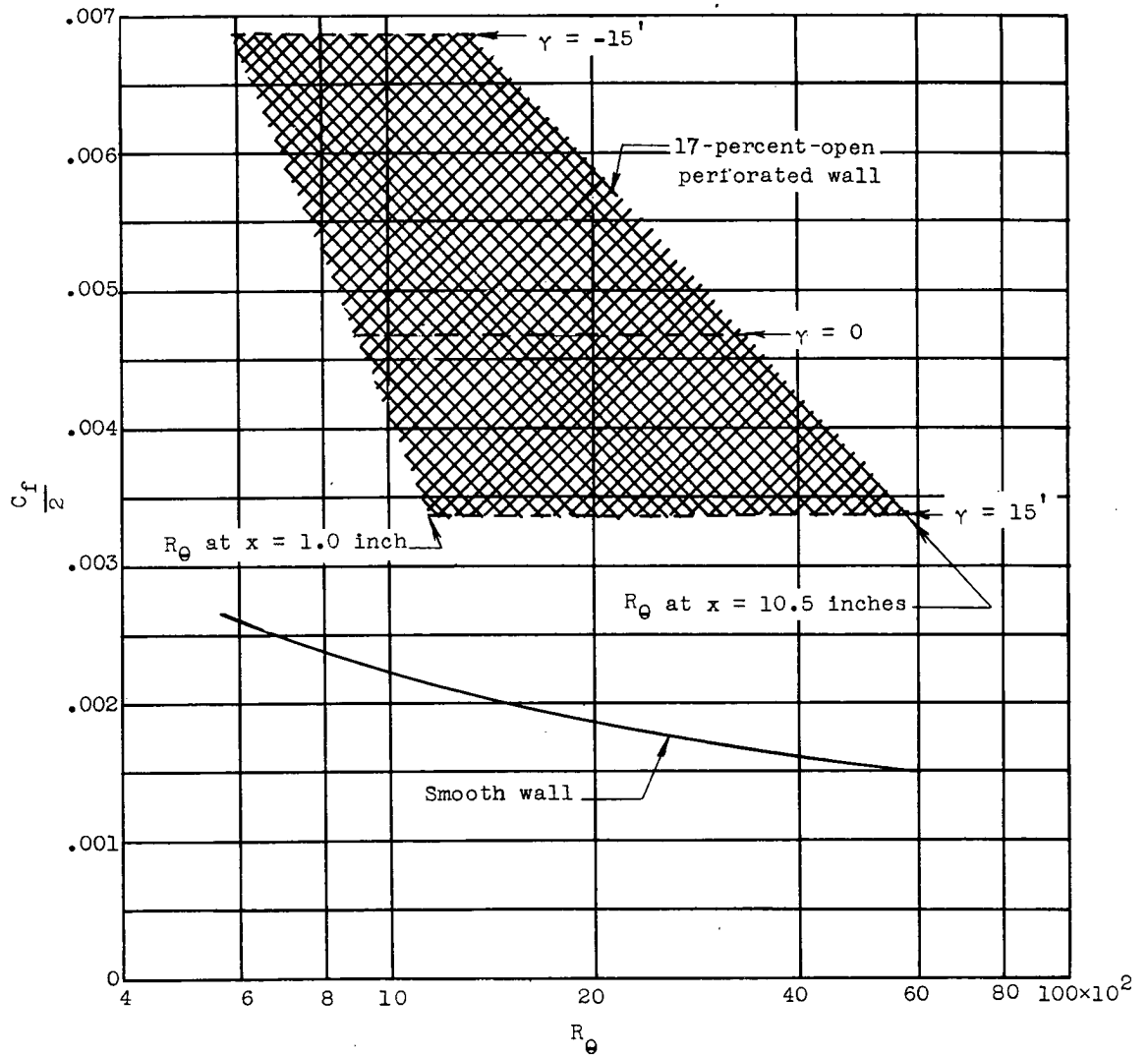


Figure 13.- A plot of the effective friction coefficients of the perforated walls compared with a smooth wall over a Reynolds number range. $M = 0.98$.

CONFIDENTIAL

CONFIDENTIAL